Shape Preferred Orientation (OCW-UN-SPO) Launeau P. 2017

UNIVERSITÉ DE NANTES
FACULTÉ DES
SCIENCES ET TECHNIQUES

Pr. Patrick Launeau
patrick.launeau@univ-nantes.fr

Image analysis of classified image define a mineral phase or class by a color code.

(see for example Launeau *et al.* 1994)

Each subset of color code can then be interpreted as an aggregate of interconnected grains. The **inertia tensor** method measure the anisotropy of the aggregate whereas the **intercepts** method can retrieve the orientation of the sub grains embedded in the aggregate.

The analysis of the sub grains by the inertia tensor method requires prior sub grain segmentation.
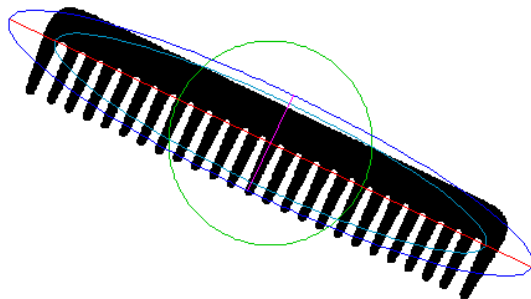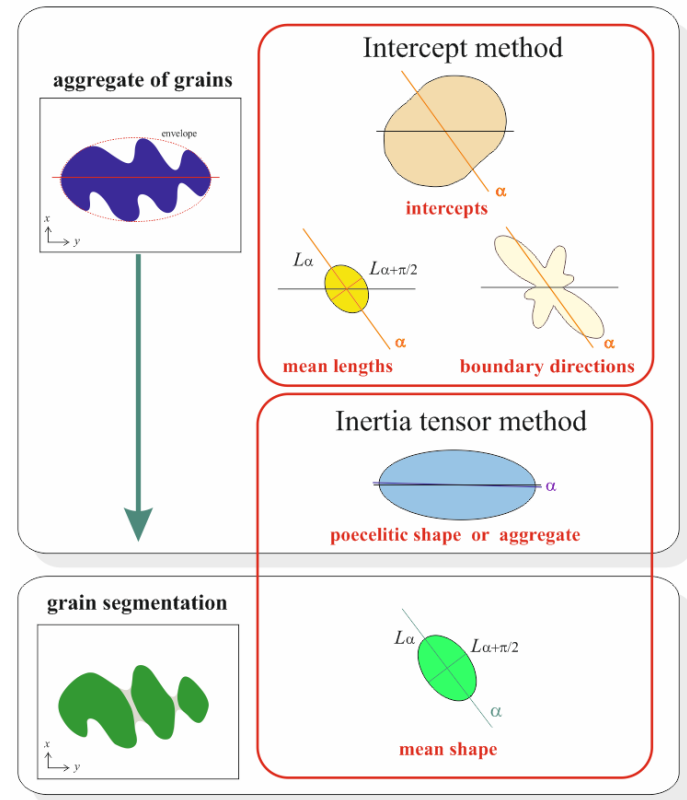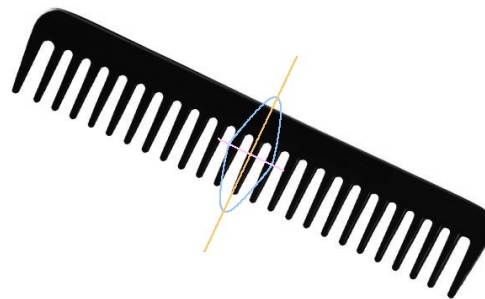
Inertia tensor Intercepts mean length boundary directions
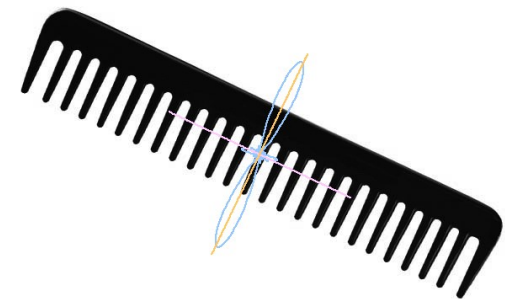
If a mineral phase is identified by a color code (yellow figure) on a digital image made of square pixels. Its subdivision in objects can be done by a scan (red line) of the neighboring pixels.

Digital image coordinate system

Connexity

4   8
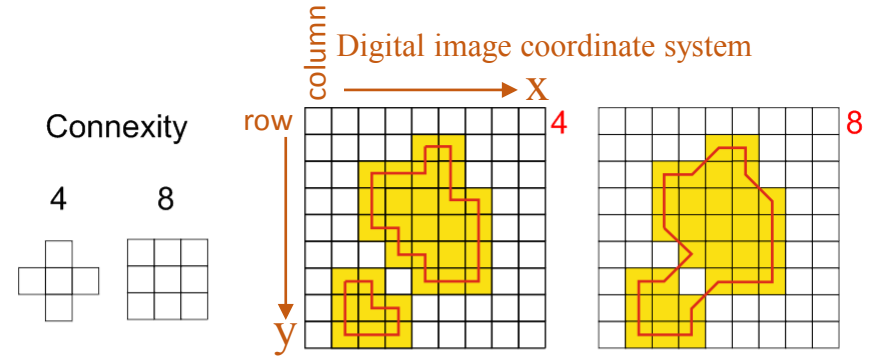
A digital scan can be done only along pixel rows and pixel columns in X and Y direction respectively. Each pixel has 4 neighbors which define the **connexity 4**.
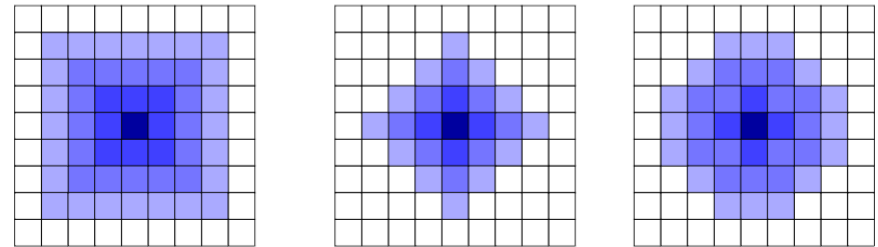
The addition of scan directions along diagonals gives a total of 8 neighbors which define the **connexity 8**. The alternation of connexity 4 and 8 is useful for the drawing of dot on digital images (see blue figures).

We will rather use the connexity 4 scan to maximize the grain segmentation. The yellow figure displays 2 objects in connexity 4 but only 1 object with 1 pixel hole in connexity 8.

3

Shape Preferred Orientation (OCW-UN-SPO) Launeau P. 2017

1) A cursor scans the digital image along rows until it find the first pixel (anchor pixel of the object) of a mineral class and attributes an object number to the same pixel coordinates in a separate layer mapping individual objects.
2) Then it tests all neighbors in connexity 4, records the position of the new neighbors belonging to the same mineral class and attributes the same object number, in the object layer, prior the transmission of their positions to the next step.
3) The loop repeats itself until the cursor reach the last pixel of the object subset of neighboring pixels encoding the object number
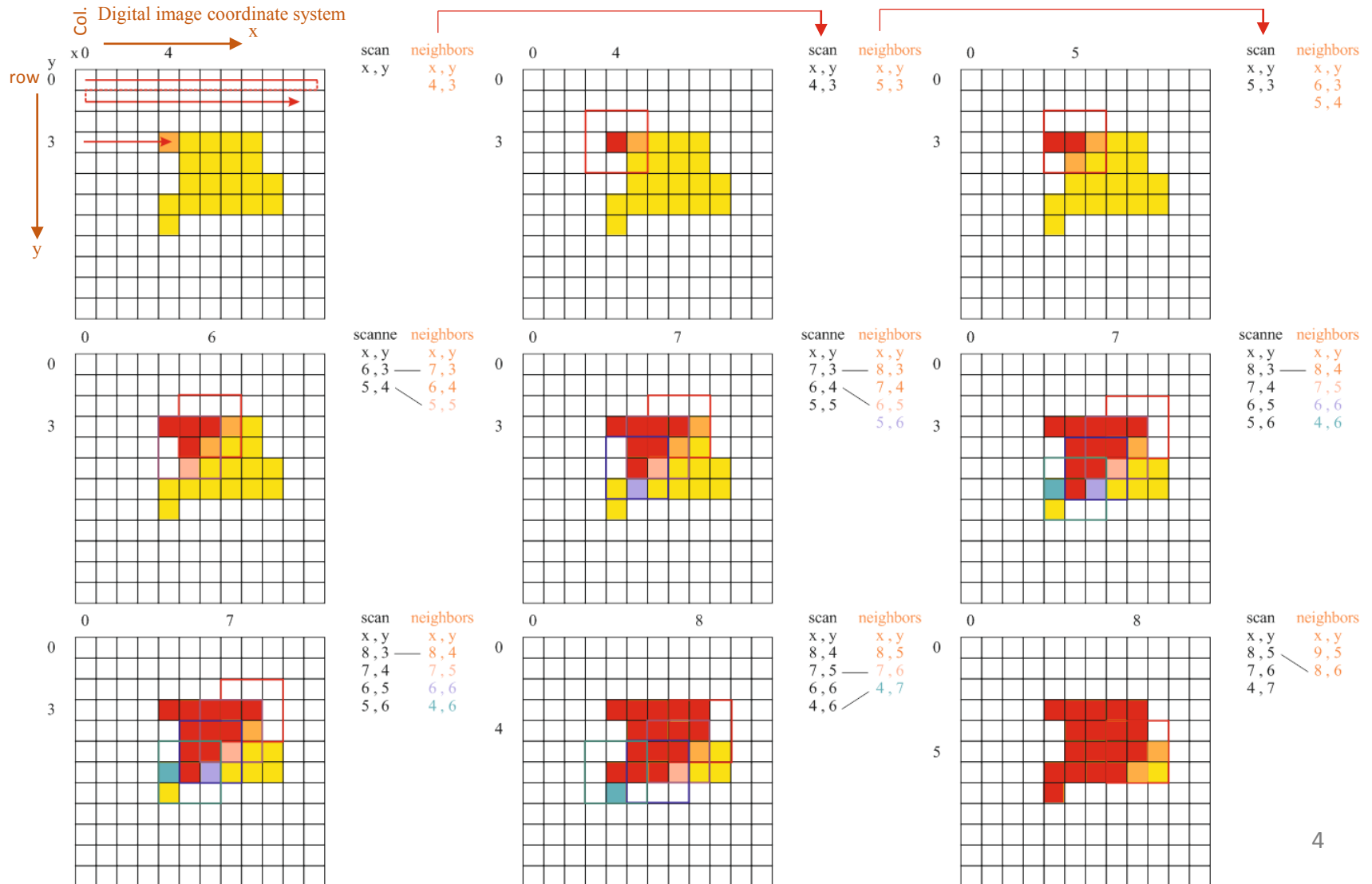
Calculation of the inertia tensor of each object identified by its first anchor pixel and its gravity center coordinates

Gravity center of the jth object:

$$x_{cj} = \frac{1}{A_j}\sum_i x_i$$

$$y_{cj} = \frac{1}{A_j}\sum_i y_i$$

Inertia tensor of the jth object:

$$m_{xxj} = \frac{1}{A_j}\sum_i (x_i - x_{cj})^2$$

$$m_{xyj} = \frac{1}{A_j}\sum_i (x_i - x_{cj})(y_i - y_{cj}) \qquad \mathbf{M}_j = \begin{vmatrix} m_{xxj} & m_{xyj} \\ m_{xyj} & m_{yyj} \end{vmatrix}$$

$$m_{yyj} = \frac{1}{A_j}\sum_i (y_i - y_{cj})^2$$

The digital image coordinate system of pixels stored in memory in rows of pixels towards the image right x with a carriage return to the next line downwards y forming columns of pixels in the digital image matrix is compatible with the clockwise standard coordinate system convention (X,Y) himself compatible with the (N,E) convention.

$$r_j = \sqrt{\frac{\mu_1}{\mu_2}}$$

Eigenvectors $R(\alpha)$ and eigenvalues $\Lambda(\mu)$ gives orientation α and shape ratio r

$$\begin{bmatrix} \mu_1 & 0 \\ 0 & \mu_2 \end{bmatrix} = \begin{bmatrix} \cos\alpha_j & \sin\alpha_j \\ -\sin\alpha_j & \cos\alpha_j \end{bmatrix} \cdot \begin{bmatrix} m_{xxj} & m_{xyj} \\ m_{xyj} & m_{yyj} \end{bmatrix} \cdot \begin{bmatrix} \cos\alpha_j & -\sin\alpha_j \\ \sin\alpha_j & \cos\alpha_j \end{bmatrix}$$

$$\Lambda = R^{-1} M R$$
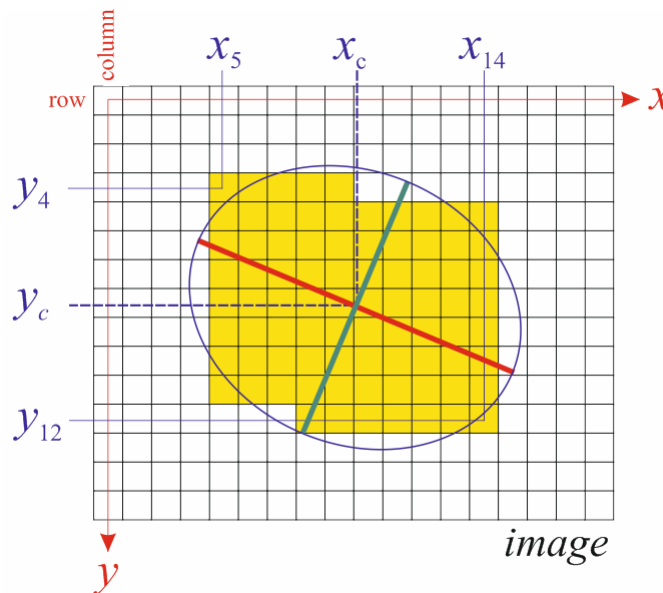
$$a_j = 2\cdot\sqrt{\mu_1}$$

$$b_j = 2\cdot\sqrt{\mu_2}$$

In practice we use the following development to speed up the calculation of the matrix elements by using only red boxes

$$m_{xxj} = \frac{1}{A}\sum_i \left(x_i - x_{cj}\right)^2 \qquad\qquad m_{xyj} = \frac{1}{A}\sum_i \left(x_i - x_{cj}\right)\left(y_i - y_{cj}\right)$$

$$m_{xxj} = \frac{1}{A}\sum_i \left(x_i^2 - 2x_i x_{cj} + x_{cj}^2\right) \qquad\qquad m_{xyj} = \frac{1}{A}\sum_i \left(x_i y_i - x_i y_{cj} - x_{cj} y_i + x_{cj} y_{cj}\right)$$

$$m_{xxj} = \frac{1}{A}\sum_i x_i^2 - \frac{2}{A}\sum_i x_i x_{cj} + \frac{1}{A}\sum_i x_{cj}^2 = \frac{1}{A}\sum_i x_i^2 - x_{cj}^2 \qquad m_{xyj} = \frac{1}{A}\sum_i x_i y_i - \frac{1}{A}\sum_i x_i \sum_i y_{cj} - \frac{1}{A}\sum_i x_{cj}\sum_i y_i + \frac{1}{A}\sum_i x_{cj}\sum_i y_{cj} = \frac{1}{A}\sum_i x_i y_i - x_{cj} y_{cj}$$

$$-\frac{2}{A}\sum_i x_i x_{cj} = -\frac{2\cdot x_{cj}}{A}\sum_i x_i = -2\cdot x_{cj}^2 \quad \frac{1}{A_j}\sum_i x_{cj}^2 = \frac{1}{A_j^2}\left(\sum_i x_{cj}\right)^2 = +x_{cj}^2$$

5

Rink (1976) and Jähne (1991).

For reason of simplification, we rather use a convention with X parallel to the N and Y parallel to the E when $\phi = \theta = \psi = 0$.

The inertia tensor can be written in the default image (X,Y) clockwise coordinate system for the jth object with surface area A_j

$$x_{jc} = \frac{1}{A_j} \sum_i x_i$$

$$y_{jc} = \frac{1}{A_j} \sum_i y_i$$

$$m_{xxj} = \frac{1}{A_j} \sum_i x_i^2 - x_c^2$$

$$m_{xyj} = \frac{1}{A_j} \sum_i x_i y_i - x_c y_c$$

$$m_{yyj} = \frac{1}{A_j} \sum_i y_i^2 - y_c^2$$

The summation of the matrix components and their division by J objects gives the mean inertia tensor giving the mean shape of the object stacking by their gravity centers.

$$\mathbf{M} = \frac{1}{J} \sum_j \mathbf{M}_j = \frac{1}{J} \begin{vmatrix} \sum_j m_{xxj} & \sum_j m_{xyj} \\ \sum_j m_{xyj} & \sum_j m_{yyj} \end{vmatrix}$$

The same eigenvector and eigenvalue procedure $\Lambda = R^{-1} M R$ gives the mean SPO intensity R and orientation α

$$\begin{bmatrix} \mu_1 & 0 \\ 0 & \mu_2 \end{bmatrix} = \begin{bmatrix} \cos\alpha & \sin\alpha \\ -\sin\alpha & \cos\alpha \end{bmatrix} \cdot \begin{bmatrix} m_{xx} & m_{xy} \\ m_{xy} & m_{yy} \end{bmatrix} \cdot \begin{bmatrix} \cos\alpha & -\sin\alpha \\ \sin\alpha & \cos\alpha \end{bmatrix}$$

$$R = \sqrt{\frac{\mu_1}{\mu_2}}$$

$$a = 2 \cdot \sqrt{\mu_1}$$
$$b = 2 \cdot \sqrt{\mu_2}$$

Stack of pixels
100%
75%
50%
25%
0%

6

Rink (1976)

Conversely, the knowledge of eigenvectors orientations R and eigenvalues intensities Λ makes possible the recalculation of the inertia tensor and their eventual weighting.

$$M = R\, \Lambda\, R^{-1}$$

$$\begin{vmatrix} m_{xxj} & m_{xyj} \\ m_{xyj} & m_{yyj} \end{vmatrix} = \begin{vmatrix} \cos\alpha_j & -\sin\alpha_j \\ \sin\alpha_j & \cos\alpha_j \end{vmatrix} \cdot \begin{vmatrix} \mu_{aj} & 0 \\ 0 & \mu_{bj} \end{vmatrix} \cdot \begin{vmatrix} \cos\alpha_j & \sin\alpha_j \\ -\sin\alpha_j & \cos\alpha_j \end{vmatrix}$$

$$\begin{vmatrix} m_{xxj} & m_{xyj} \\ m_{xyj} & m_{yyj} \end{vmatrix} = \begin{vmatrix} \mu_{aj}\cdot\cos^2\alpha_j + \mu_{bj}\cdot\sin^2\alpha_j & \left(\mu_{aj}-\mu_{bj}\right)\cdot\cos\alpha_j\cdot\sin\alpha_j \\ \left(\mu_{aj}-\mu_{bj}\right)\cdot\cos\alpha_j\cdot\sin\alpha_j & \mu_{aj}\cdot\sin^2\alpha_j + \mu_{bj}\cdot\cos^2\alpha_j \end{vmatrix}$$

For the inertia tensor:

$$a_j = 2\cdot\sqrt{\mu_{aj}}$$
$$b_j = 2\cdot\sqrt{\mu_{bj}}$$

$\longrightarrow$

$$\mu_{aj} = a_j^2/4$$
$$\mu_{bj} = b_j^2/4$$

Substituting μ_a and μ_b by the inertia tensor diagonal components gives an inertia tensor proportional to the area of each object

$$\mathbf{M}_{Tj} = \frac{1}{4}\cdot\begin{bmatrix} a_j^2\cdot\cos^2\alpha_j + b_j^2\cdot\sin^2\alpha_j & \left(a_j^2-b_j^2\right)\cdot\cos\alpha_j\cdot\sin\alpha_j \\ \left(a_j^2-b_j^2\right)\cdot\cos\alpha_j\cdot\sin\alpha_j & a_j^2\cdot\sin^2\alpha_j + b_j^2\cdot\cos^2\alpha_j \end{bmatrix}$$

Its division by the area Aj of each object gives the same weight to each object

$$\mathbf{M}_{Tj} = \frac{1}{4\cdot A_j}\cdot\begin{bmatrix} a_j^2\cdot\cos^2\alpha_j + b_j^2\cdot\sin^2\alpha_j & \left(a_j^2-b_j^2\right)\cdot\cos\alpha_j\cdot\sin\alpha_j \\ \left(a_j^2-b_j^2\right)\cdot\cos\alpha_j\cdot\sin\alpha_j & a_j^2\cdot\sin^2\alpha_j + b_j^2\cdot\cos^2\alpha_j \end{bmatrix}$$ with $A_j = \pi\cdot a_j\cdot b_j$

Launeau (2004), Launeau & Robin (2005).

7

The inertia tensor $\mathbf{M}_{Tj}$ resulting of the scan pixel by pixel through out the whole surface of each object it is weighted by its area. A normalization of each object to its area gives the same weight to each object.

Inertia tensor

Normalized tensor

Inverse tensor of ellipse

$$\frac{1}{l_\psi^2} = \frac{1}{l_{ellipse\,\psi}^2} = \frac{\cos^2 \psi}{a^2} + \frac{\sin^2 \psi}{b^2}$$

Pixel density
100%
75%
50%
25%
0%

Inertia tensor
Ellipse of A
Disk of A
α direction
$\alpha\perp$ direction

True ellipse radius l

$$l_\psi = \frac{1}{\sqrt{\dfrac{\cos^2 \psi}{a^2} + \dfrac{\sin^2 \psi}{b^2}}}$$

Proportional to the area

Unweighted

Proportional to 1 / area

Rink (1976)

If $A_j = 1$

If $A_j = \pi \cdot a_j \cdot b_j$

If $A_j = 1$

$$\mathbf{M}_{Tj} = \frac{1}{4 \cdot A_j} \begin{bmatrix} a_j^2 \cdot \cos^2 \alpha_j + b_j^2 \cdot \sin^2 \alpha_j & \left(a_j^2 - b_j^2\right) \cdot \cos \alpha_j \cdot \sin \alpha_j \\ \left(a_j^2 - b_j^2\right) \cdot \cos \alpha_j \cdot \sin \alpha_j & a_j^2 \cdot \sin^2 \alpha_j + b_j^2 \cdot \cos^2 \alpha_j \end{bmatrix}$$

$$\mathbf{M}_{Ej} = A_j \cdot \begin{bmatrix} \dfrac{1}{a_j^2} \cdot \cos^2 \alpha_j + \dfrac{1}{b_j^2} \cdot \sin^2 \alpha_j & \left(\dfrac{1}{a_j^2} - \dfrac{1}{b_j^2}\right) \cdot \cos \alpha_j \cdot \sin \alpha_j \\ \left(\dfrac{1}{a_j^2} - \dfrac{1}{b_j^2}\right) \cdot \cos \alpha_j \cdot \sin \alpha_j & \dfrac{1}{a_j^2} \cdot \sin^2 \alpha_j + \dfrac{1}{b_j^2} \cdot \cos^2 \alpha_j \end{bmatrix}$$

Ellipse inverse tensors $\mathbf{M}_{Ej}$ are weighted by the inverse of the area. A multiplication of each inverse tensor of ellipse by its area gives the same weight to each object.
The comparison between those 3 tensors allows the detection of size effects on the SPO calculation.

Launeau (2004), Launeau & Robin (2005).

If the inertia tensor basically counts along a scanline the number of pixels belonging to a mineral phase or class the **intercepts method** only counts each time a scanline cursor get out of the mineral class. This event corresponds to the successive detection of a pixel in and out of the mineral class. Moreover the intercepts method rotates the net of parallel scanlines in all directions with a constant angular step.

The summation of the intercepts counts in all directions draws a **rose diagram of intercepts** in which the minimum count indicates the direction of elongation of the sub grains, hidden in the aggregate but revealed by the aggregate boundaries.

$\alpha = 90°$ $N_1(j,90°)$:

$N_1(90°) = 9$ intercepts

Rose

$\alpha = 145°$

$\alpha = 0°$ to $180°$ α_{min}

$N_1(145°) = 7$ intercepts
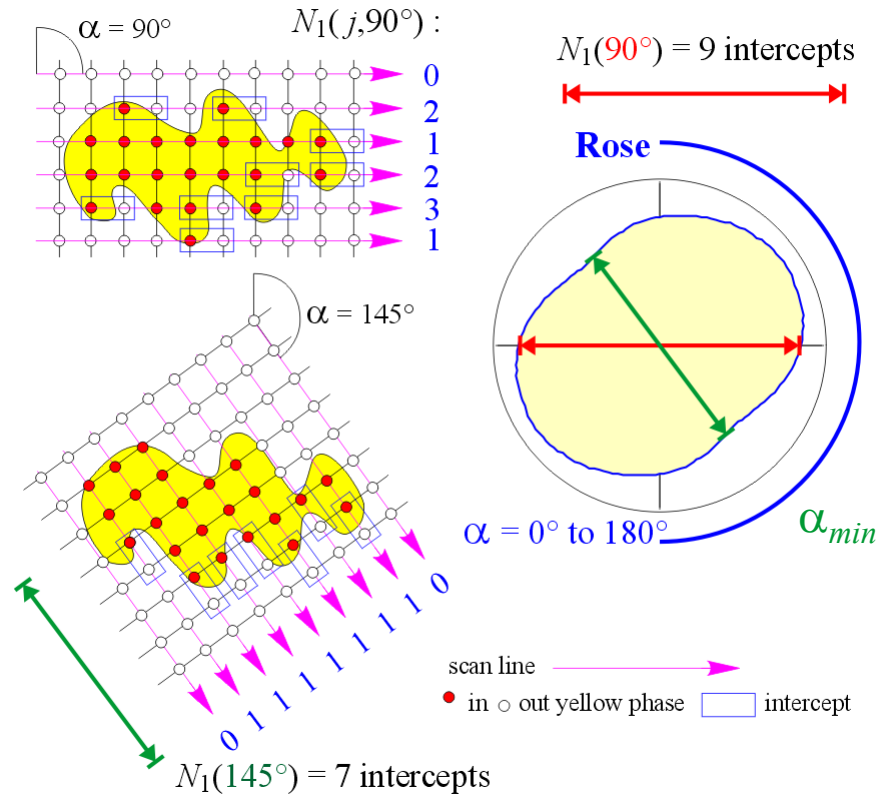
The intercepts counting being done in 1D along scanlines it is recorded as N_1 or N_L per angle of analysis.

scan line
● in ○ out yellow phase ▢ intercept

$\alpha = 90°$ $N_1(j,90°)$:
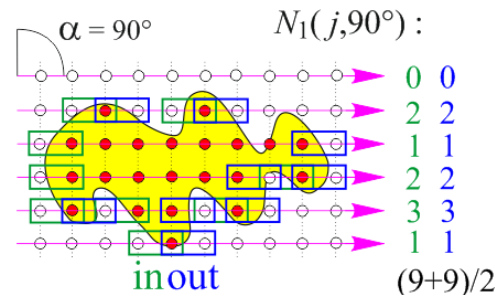
In practice it is safer (in case of noise) to count intercepts in and out the object and to divide the sum by 2.

in out $(9+9)/2$

Saltykov (1958), Underwood (1970), Serra (1982), Panozzo (1983), Coster &Chermant (1989), Launeau (1990).

The sum of the counts in the direction of analysis is the intercepts count. It is also the projection of the mineral class on a perpendicular direction also called total diameter D.

The area being the count of pixels belonging to the mineral class the division of the area by the count of intercepts gives directly the mean length L of the segments intercepted or traversed by the net of scanlines.

The rose diagrams of intercepts counts and projections cannot be combined with other 2D sections in 3D which is the main interest of the **mean intercepts length rose diagram** also called traverses rose diagram.

counts $\qquad N_1(90°) = 9$ intercepts

1 unit $\qquad N_1(j, 90°)$:

$$\begin{array}{c} 0 \\ 2 \\ 1 \\ 2 \\ 3 \\ 1 \end{array}$$

projection (total diameter)

$D(90°) = 9$ units

1 unit

$$\begin{array}{c} 1 \quad 1 \\ 8 \\ 6 \quad 1 \\ 1 \quad 2 \quad 1 \\ 1 \end{array}$$

mean length
22 units / 9 segments = 2.4 units per segment

$L(90°) = 2.4$ units

Roses :

counts $\qquad$ projection $\qquad$ mean length
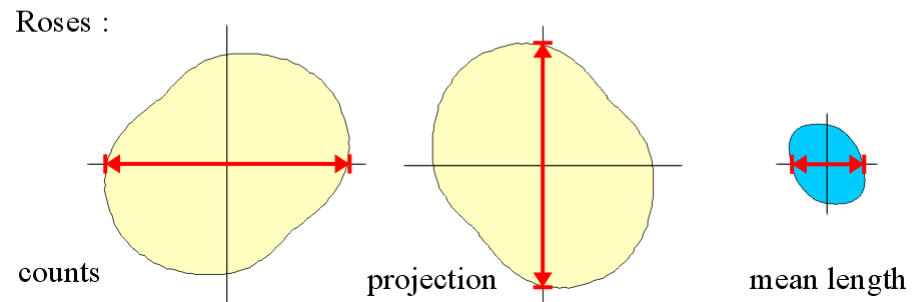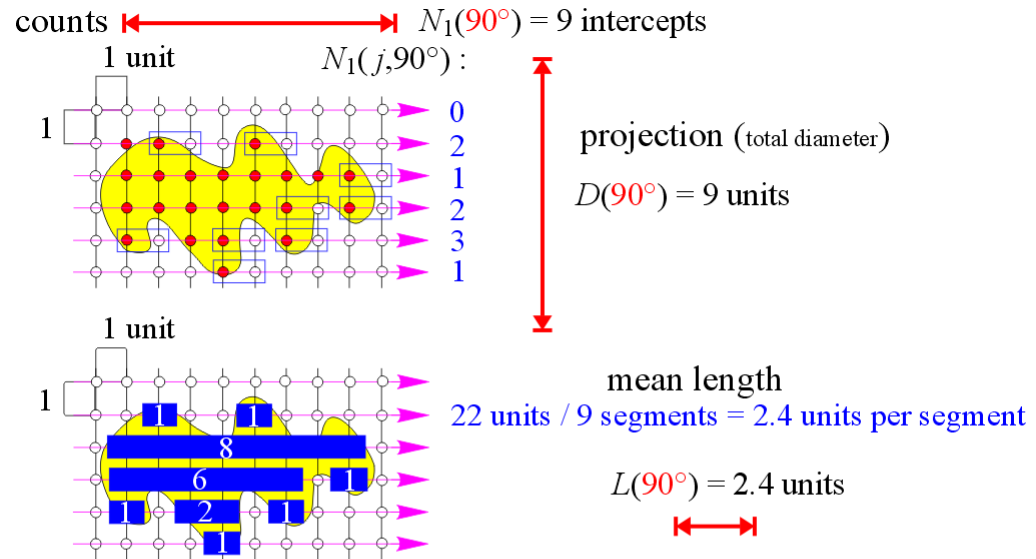
Launeau & Robin (1996)
See also mean free length Underwood (1970)

The intercepts method is only sensitive to the angular distribution of the boundaries. It is therefore absolutely necessary to establish that the set of boundaries can effectively retrieve the orientation of sub grains forming an aggregate. Blind application of the method is dangerous and can produce meaningless results.

Theoretical shapes of roses
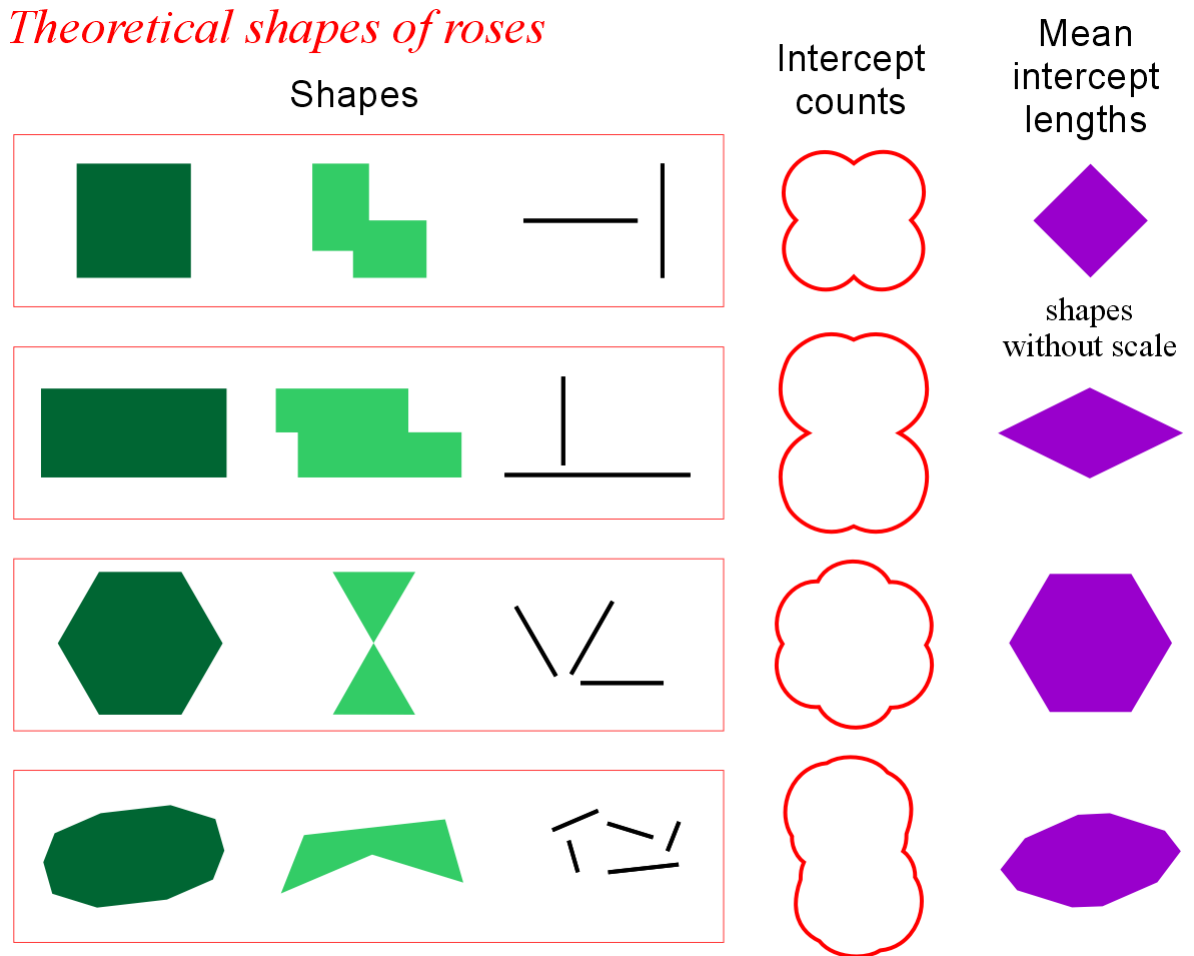
Notes that intercepts rose diagrams are always centrosymmetric. Triangles with uneven distributions of 3 boundaries produce a rose diagram of even distributions of 6 borders. All uneven symmetry orders are null.

Launeau & Robin (1996)

11

A digital image has 4 directions of counting pixel per pixel in line and column and 4 more ones in diagonal with $2^{0.5}$ pixel steps.

The use of narrower angular step required a resampling of the digital image in each scanline direction with a constant counting step. Then a scanline tangent to a border made of square pixels displays many unexpected outputs of objects.

A weighted low-pass filter allowing the calculation of pixel densities along each scanline local outputs of objects are smoothed out and the right count of intercepts is found at 50% pixel density.
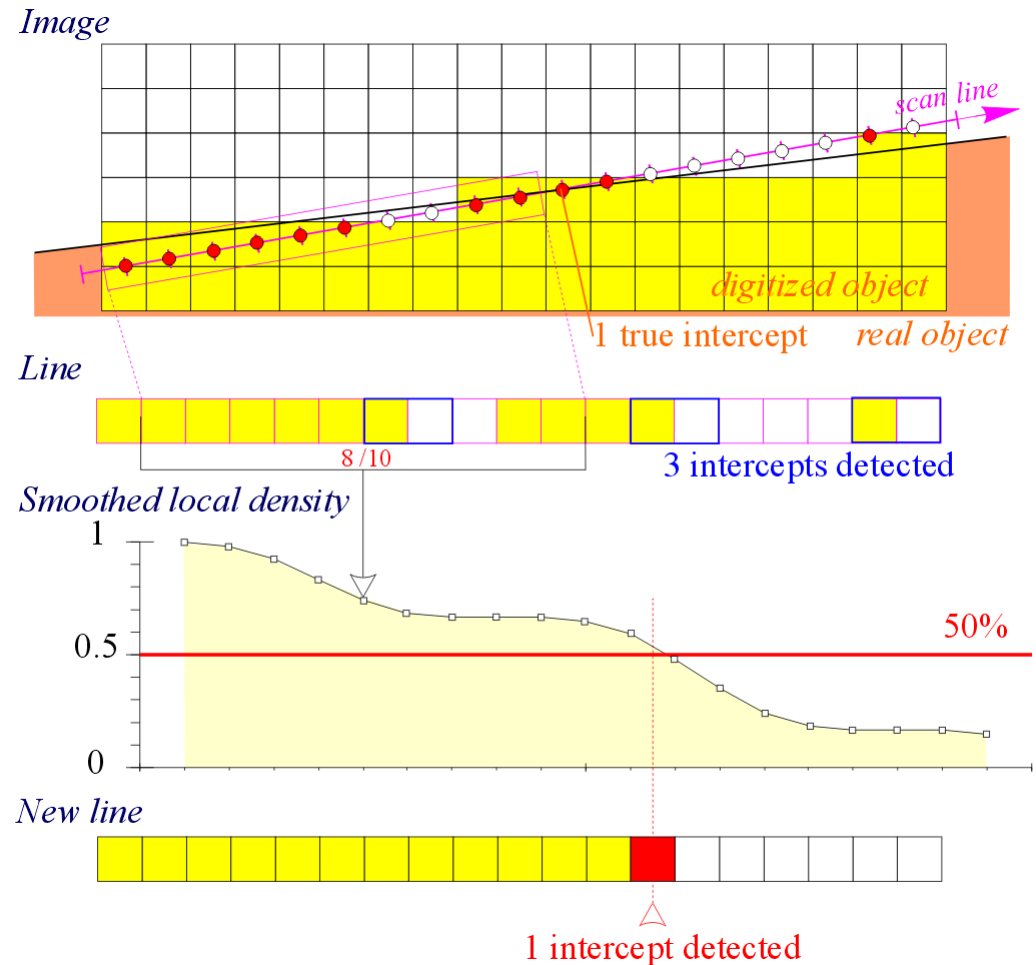
Low pass coefficient: 1 3 6 8 9 9 8 6 3 1

Image

scan line

digitized object

1 true intercept   *real object*

Line

8 /10

3 intercepts detected

Smoothed local density

1

0.5

0

50%

New line

1 intercept detected

Launeau & Robin (1996)   12

The comparison between raw counts of intercepts in red with the low-pass filter allowing the count of intercepts on pixel densities in blue evidences the interest of such counting procedure.

Further filter however can help to minimize the noise.

Launeau & Robin (1996)

See also for digital anisotropy
Panozzo Heilbronner (1988).

Image tested

Counts

Without low-pass

With low-pass
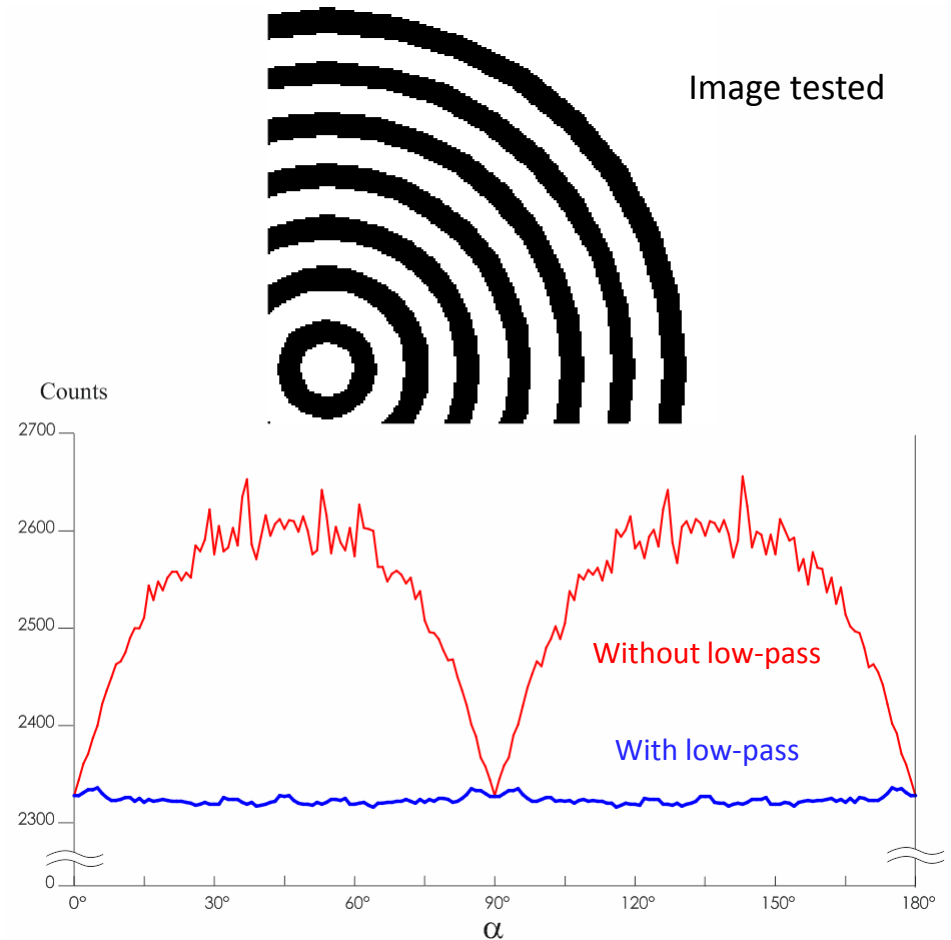
Angular distribution of the intercepts counts

Rink (1976)

The drawing of the **mean intercepts length** with a constant angular step of 2° is a rose diagram equivalent to the drawing of an ellipse presented in course 3 p. 10. Thus, the first eigenvector gives the orientation α and the square root of the eigenvalues ratio gives the SPO intensity R.
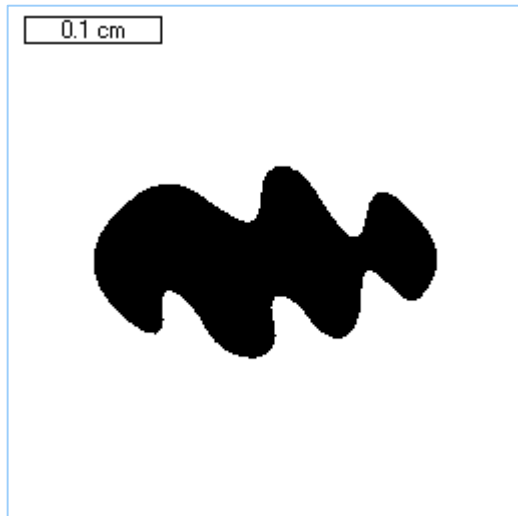
The size of the best fitting ellipse is given by a_{Lc} and b_{Lc}

$$a_{Lc} = \left(2\mu_1 \cdot \mu_1^{0,5}/\mu_2^{0,5}\right)^{0,5} \qquad a_{Lc} = \left(2\mu_1^{1,5}/\mu_2^{0,5}\right)^{0,5}$$

$$b_{Lc} = \left(2\mu_2 \cdot \mu_2^{0,5}/\mu_1^{0,5}\right)^{0,5} \qquad b_{Lc} = \left(2\mu_2^{1,5}/\mu_1^{0,5}\right)^{0,5}$$

But the square root of the eigenvalues ratio gives directly R

$$R = \sqrt{\frac{\mu_1}{\mu_2}} = \frac{a_{Lc}}{b_{Lc}}$$

Launeau (2004)

0.1 cm

inertie : a=0.1166 cm b=0.0884 cm R=1.319 , 144.20°
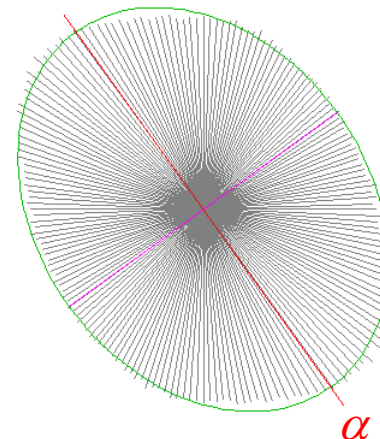
Mean length Traverses

Compare with p. 19

1.319 @ 144.2°

α

0.1 cm

Fourier series are particularly suitable for the analysis of centrosymmetric intercepts rose diagrams presenting only even phases. Uneven phases are always null.

The intercepts count N_L in one direction α is the summation of the counts made along the J scanlines.

$$N_L(\alpha) = \sum_j N_L(j, \alpha)$$

It can be decomposed in M or $2m$ even harmonics as cosines A and sinus B series. $\alpha = (k \cdot \delta\alpha)$ is the direction of analysis and $K = 180°/\delta\alpha$ is the number of directions.

$$A_{2m} = \frac{2}{K} \sum_{k=0}^{K-1} N_L(k \cdot \delta\alpha) \cos(2m \cdot k \cdot \delta\alpha)$$

$$B_{2m} = \frac{2}{K} \sum_{k=0}^{K-1} N_L(k \cdot \delta\alpha) \sin(2m \cdot k \cdot \delta\alpha)$$

The phase angle φ_M of the Fourier series is proportional to the arc tangent of A/B and the power of the series is given by the square root of the sum of the square of A and B:

$$\varphi_{2m} = \frac{1}{2m} \cdot \arctan\left(\frac{B_{2m}}{A_{2m}}\right)$$

$$C_{2m} = \sqrt{A_{2m}^2 + B_{2m}^2}$$

It is then possible to rebuilt the intercepts rose diagram by the progressive addition of harmonics

$M=0, m=0 \rightarrow \quad F_0(\alpha) = C_0$

$M=2, m=1 \rightarrow \quad F_2(\alpha) = C_0 + C_2 \cos 2(\alpha - \varphi_2)$

$M=4, m=2 \rightarrow \quad F_4(\alpha) = C_0 + C_2 \cos 2(\alpha - \varphi_2) + C_4 \cos 4(\alpha - \varphi_4)$

$M=6, m=3 \rightarrow \quad F_6(\alpha) = C_0 + C_2 \cos 2(\alpha - \varphi_2) + C_4 \cos 4(\alpha - \varphi_4) + C_6 \cos 6(\alpha - \varphi_6)$

with $A_0 = C_0 = \frac{1}{K} \sum_{k=0}^{K-1} N_L(k \cdot \delta\alpha)$

$$F_M(\alpha) = C_0 + \sum_{m=1}^{M/2} C_{2m} \cos 2m(\alpha - \varphi_{2m})$$

or

$$F_M(\alpha) = C_0 + \sum_{m=1}^{M/2} \left(A_{2m} \cdot \cos(2m \cdot \alpha) + B_{2m} \cdot \sin(2m \cdot \alpha) \right)$$

Hilliard (1962)
Launeau & Robin (1996)

15

The harmonic 0 (C_0) corresponds to the mean intercepts count. It is the best circle pathing by the intercepts counts rose diagram. The counting interval along scanlines times an intercepts count may gives a metric size (cm in the present example).

M = 0
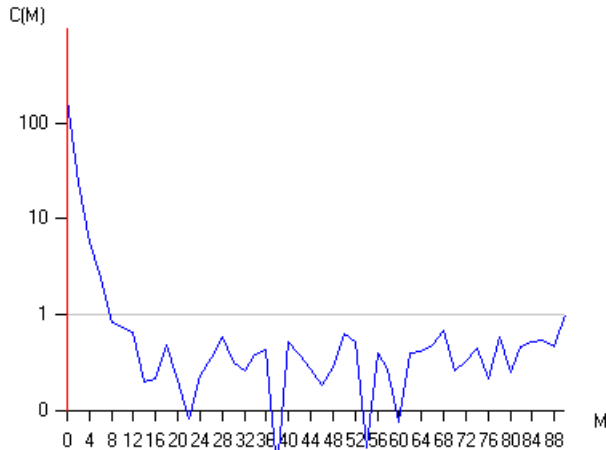
$$C_0 = \overline{N}_L(\alpha)$$

M = 0

$$F_0(\alpha) = C_0$$

$$F_M(\alpha) = C_0 + \sum_{m=1}^{M/2} C_{2m} \cos 2m(\alpha - \varphi_{2m})$$

16
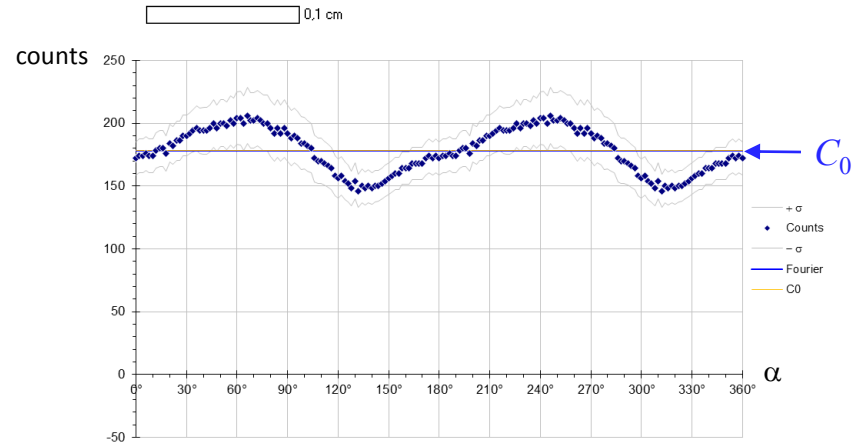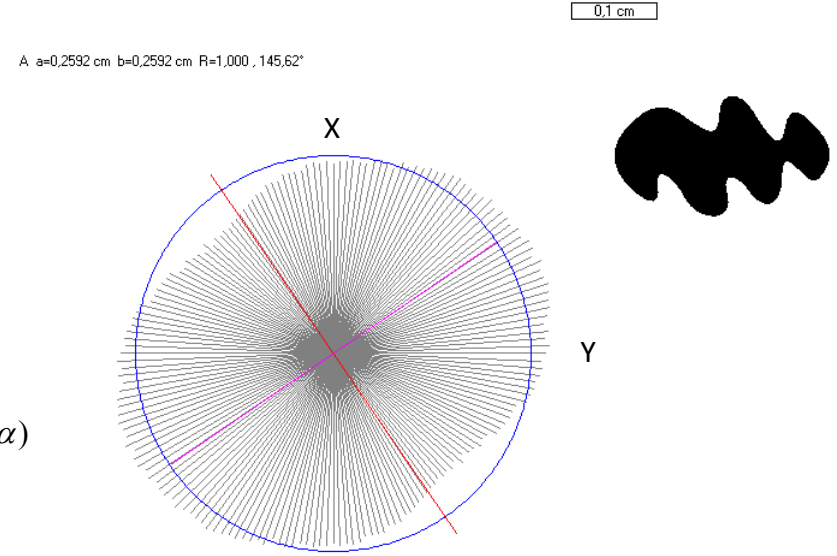
The harmonic 2 corresponds to the best ellipse pathing by the intercepts rose diagram. The SPO direction is therefore given by the phase angle of the 2nd harmonic φ_2.
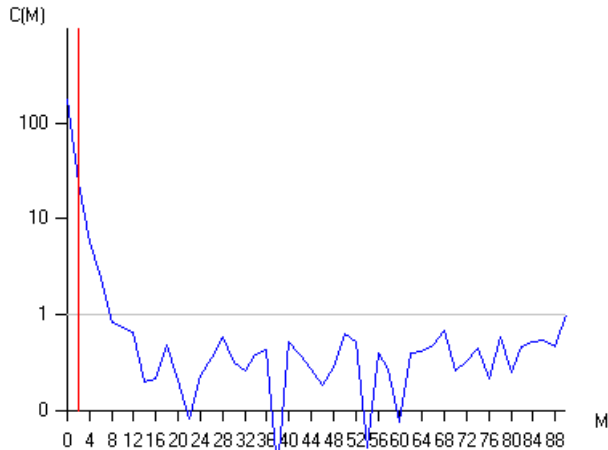
0,1 cm

A a=0,2942 cm b=0,2242 cm R=1,312 , 145,62°

$\alpha = \varphi_2$

M = 2

M = 2

$$F_2(\alpha) = C_0 + C_2 \cos 2(\alpha - \varphi_2)$$

C(M)

$$F_M(\alpha) = C_0 + \sum_{m=1}^{M/2} C_{2m} \cos 2m(\alpha - \varphi_{2m})$$

0,1 cm

counts

$C_0 + C_2$

+ σ
Counts
− σ
Fourier
C2

α

C_2

φ_2
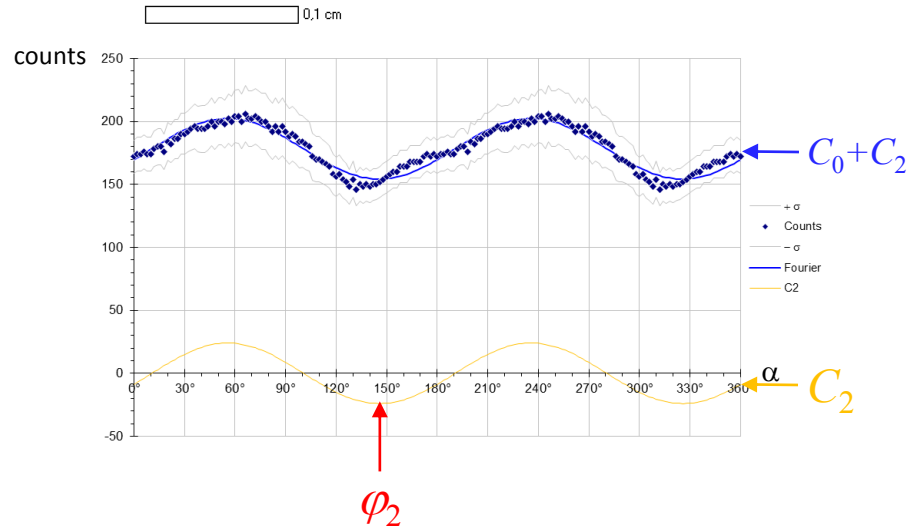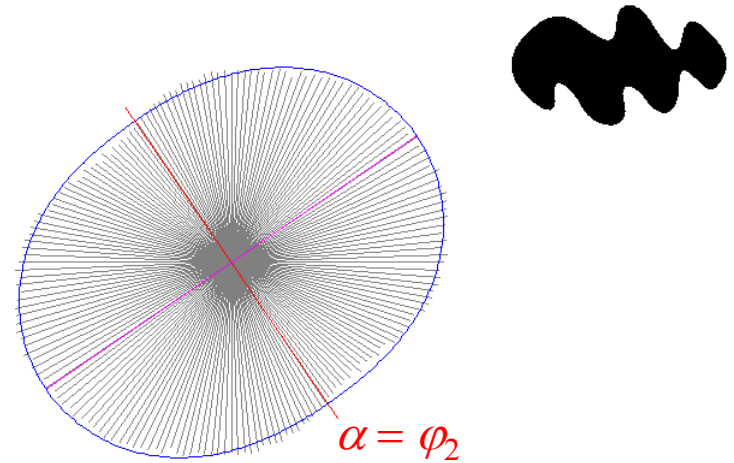
The harmonic 8 is the last one before the blank noise. It corresponds to the best shape fitting the intercepts rose diagram. The SPO intensity is the ratio of the intercepts counts found in α and $\alpha+90°$ directions

0,1 cm

A a=0,2924 cm b=0,2212 cm R=1,322 , 145,62°

α

M = 8

M = 8

$$F_8(\alpha) = C_0 + C_2 \cos 2(\alpha - \varphi_2) + C_4 \cos 4(\alpha - \varphi_4) + C_6 \cos 6(\alpha - \varphi_6) + C_8 \cos 8(\alpha - \varphi_8)$$

C(M)

100

10

1

Blank noise

0

0 4 8 12 16 20 24 28 32 36 40 44 48 52 56 60 64 68 72 76 80 84 88   M

$$F_M(\alpha) = C_0 + \sum_{m=1}^{M/2} C_{2m} \cos 2m(\alpha - \varphi_{2m})$$

0,1 cm

counts 250

200

150

100

50

0

-50

6° 30° 60° 90° 120° 150° 180° 210° 240° 270° 300° 330° 360°

+σ
Counts
−σ
Fourier
C8

$C_0 + C_2 + C_4 + C_6 + C_8$

α

C_8

18
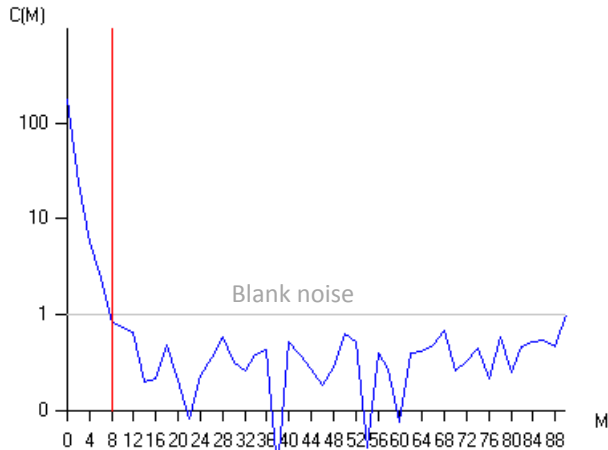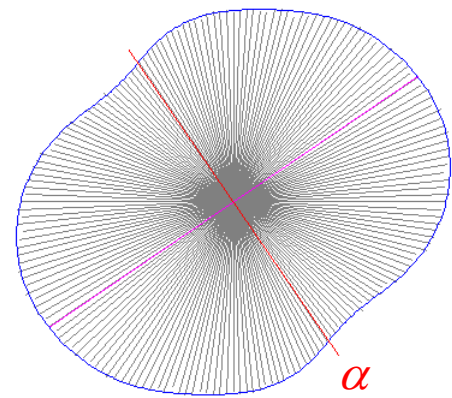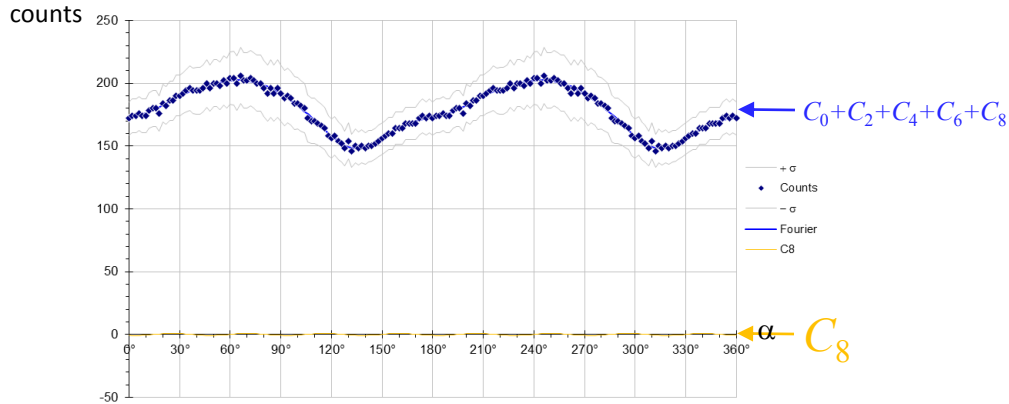
The division of the mineral class by the intercept counts in each angle of analysis gives the mean length intercepts or traverses rose diagram:

$$\bar{L}(\alpha) = \frac{A}{J\,N_L(\alpha)} = I\,\frac{N_0}{N_1(\alpha)}$$

I sampling interval on line
J interline

The shape ratio remain the same.

M = 8

M = 8

α

Intercepts

A a=0,2924 cm b=0,2212 cm R=1,322 , 145,62°
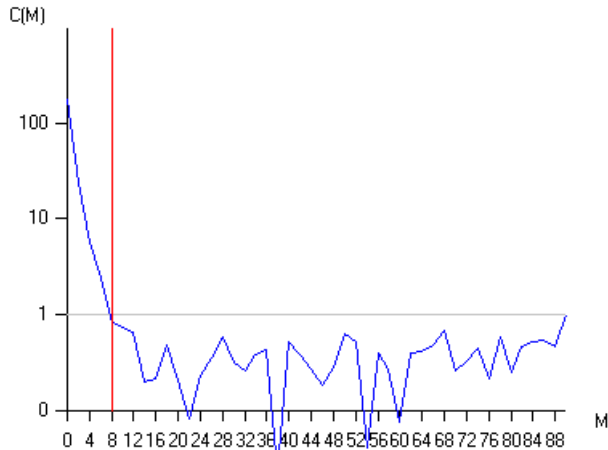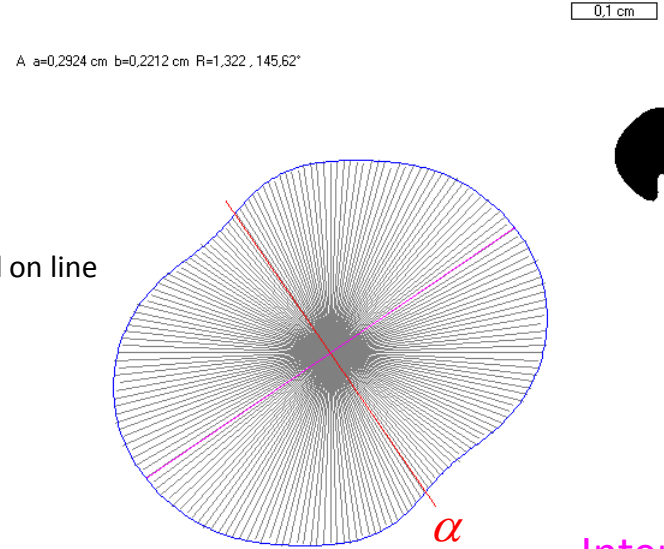
A a=0,1171 cm b=0,0886 cm R=1,322 , 145,62°

0,1 cm

C(M)

100

10

1

0

0 4 8 12 16 20 24 28 32 36 40 44 48 52 56 60 64 68 72 76 80 84 88   M

$$F_M\,(\alpha)\;=\;C_0\;+\;\sum_{m=1}^{M/2} C_{2m}\;\cos 2m(\alpha - \varphi_{2m})$$
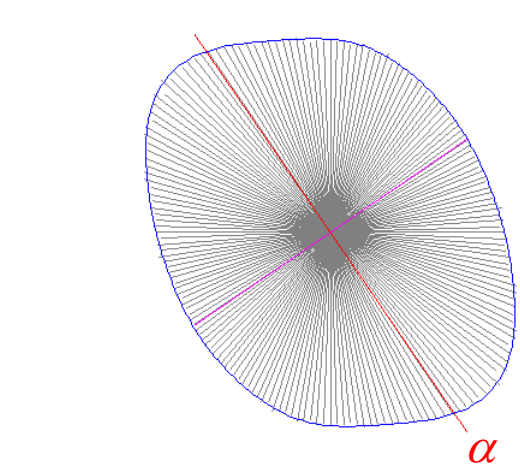
Mean length Traverses

Compare with p. 14

1.322 @ 145.6°

α

0,1 cm

A rose of directions can be extracted from the second derivative of the intercepts rose, we will not develop further the method in this course.

For one rod :

$$D(\alpha) \;=\; L\,|\sin(\alpha - \psi)| \;=\; \frac{L}{\sqrt{2}}\,\sqrt{1 - \cos 2(\alpha - \psi)}$$

$$D(\alpha) + D''(\alpha) = 0 \quad \text{for } \alpha \neq \psi \text{ modulo } \pi$$
$$\infty \quad \text{for } \alpha = \psi \text{ modulo } \pi$$

Since the first derivative $D'(\alpha)$ changes from $-L$ to $+L$ on either side of the singularity, $D(\alpha) + D''(\alpha)$ for one rod is a Dirac 'function', $2\,L\,\delta(\alpha - \psi)$, i.e. with an integrated value of $2\,L$:

$$D(\alpha) + D''(\alpha) = 2\,L\,\delta(\alpha - \psi)$$

For a population of rods :

$$N_L(\alpha) = \frac{D(\alpha)}{A^w} = \frac{1}{A^w}\sum_{i=1}^{P} L^i \left| \sin(\alpha - \psi^i) \right|$$

$$N_L(\alpha) + N_L''(\alpha) = \frac{2}{A^w}\sum_{i=1}^{P} L^i\, \delta(\alpha - \psi^i)$$

Intercepts rose diagram of a rod L
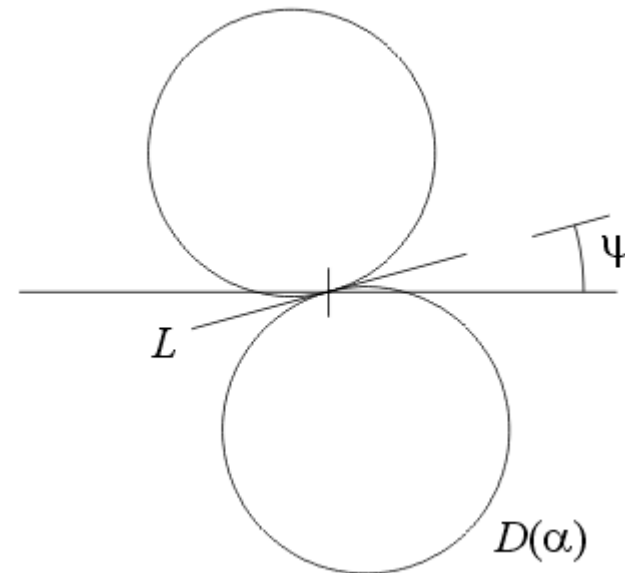
ψ

L

$D(\alpha)$

Hilliard (1962)
Launeau & Robin (1996)

A rose of directions can be extracted from the second derivative of the intercepts rose, we will not develop further the method in this course.

For a population of rods :

$$N_L(\alpha) = \frac{D(\alpha)}{A^w} = \frac{1}{A^w} \sum_{i=1}^{P} L^i \left| \sin(\alpha - \psi^i) \right|$$

$$N_L(\alpha) + N_L''(\alpha) = \frac{2}{A^w} \sum_{i=1}^{P} L^i \, \delta(\alpha - \psi^i)$$

M = 8

C(M)
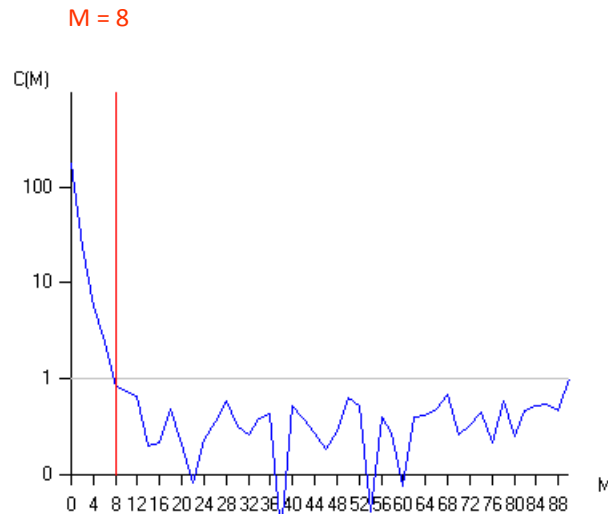
$$N_L''(\alpha) \approx F_M''(\alpha) = - \sum_{m=1}^{M/2} (2m)^2 \left(A_{2m} \cos 2m\alpha + B_{2m} \sin 2m\alpha \right)$$

$$\frac{2\,l(\alpha)}{A^w} \approx F_M(\alpha) + F_M''(\alpha) = C_0 + \sum_{m=1}^{M/2} \left[1 - (2m)^2 \right] \left(A_{2m} \cos 2m\alpha + B_{2m} \sin 2m\alpha \right)$$

A Nla=2,069 cm⁻¹ Nlb=2,735 cm⁻¹ R=1,322 , 145,62° , angle X: 124,38°

0,1 cm

(1) 134°
(2) 10°
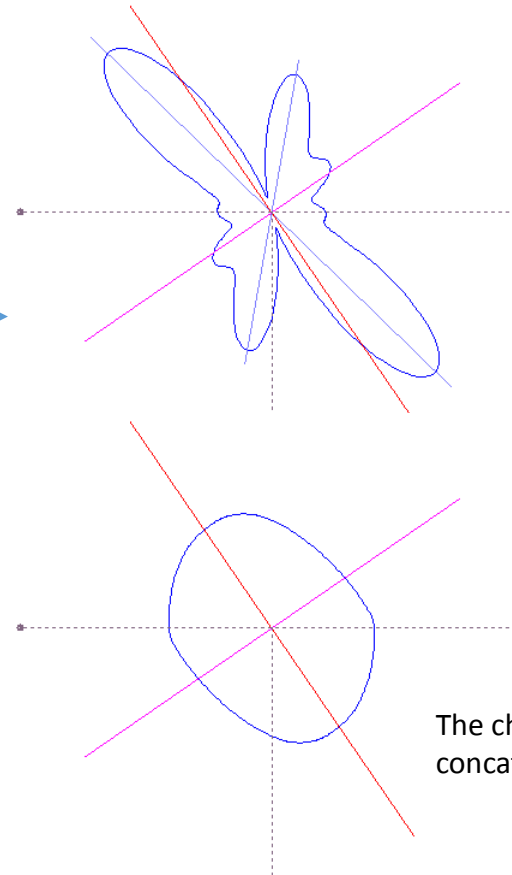
The characteristic shape is a concatenation of directions

Hilliard (1962)
Launeau & Robin (1996)

21

An excess of harmonic integration in the Fourier reconstruction only add noise which conduct to the detection of the pixel geometry and aberrant rose of directions.

Mean length traverses

A a=0,1174 cm b=0,0893 cm R=1,315 , 145,62° , angle X: 124,38°

(1) 127°
(2) 134°
(3) 141°
(4) 168°
(5) 177°
(6) 9°

M = 54

blank noise

Directions

A Nla=2,064 cm⁻¹ Nlb=2,716 cm⁻¹ R=1,315 , 145,62° , angle X: 124,38°

(1) 91°
(2) 99°
(3) 106°
(4) 119°
(5) 127°
(6) 134°
(7) 141°
(8) 148°
(9) 155°
(10) 162°
(11) 169°
(12) 2°
(13) 10°
(14) 18°
(15) 25°
(16) 32°
(17) 40°
(18) 56°
(19) 64°
(20) 70°
(21) 84°
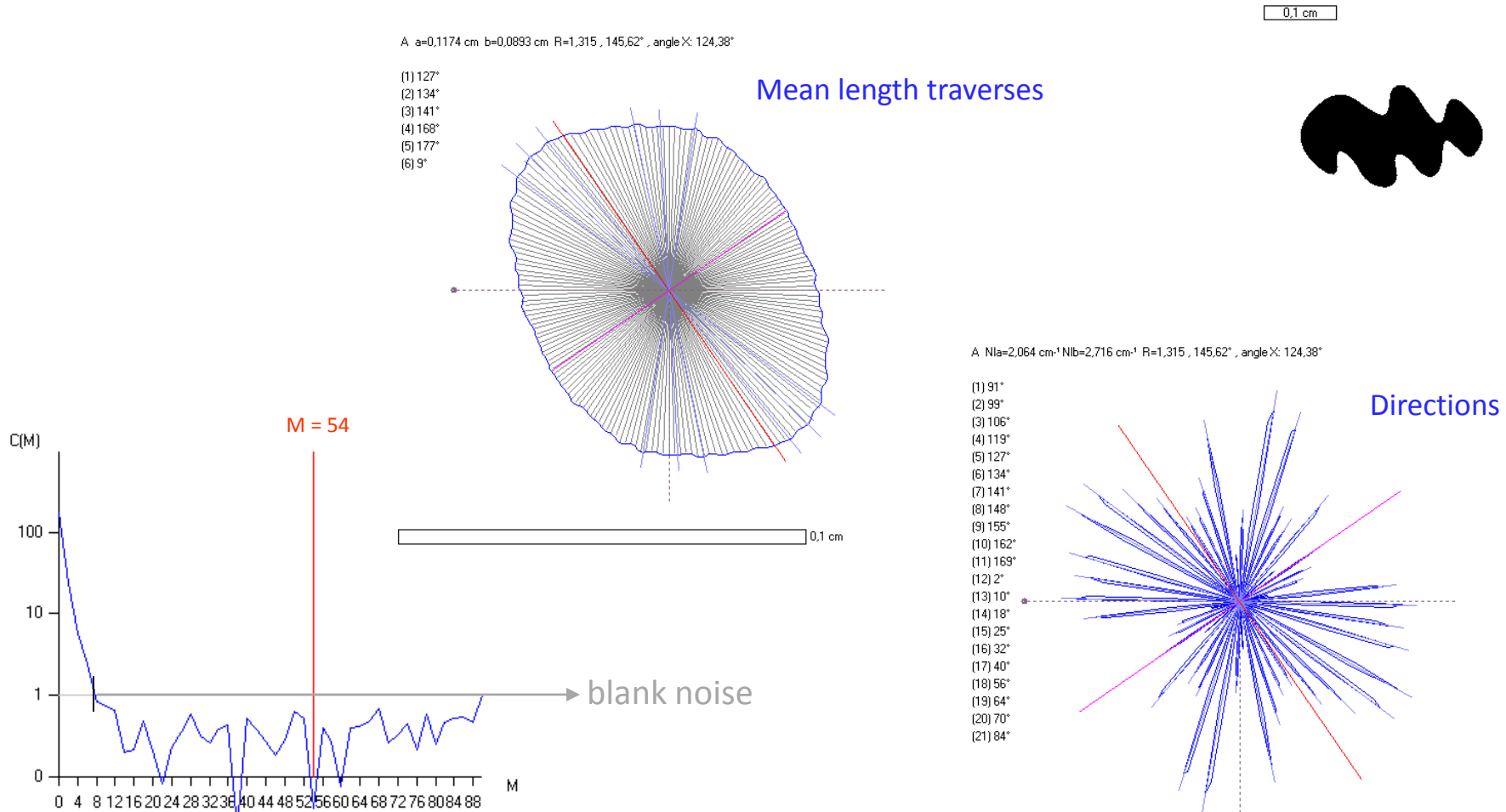
The power spectrum allows the analysis of the object boundaries symmetry by the detection of periodic distribution of C.

C_2 = anisotropy
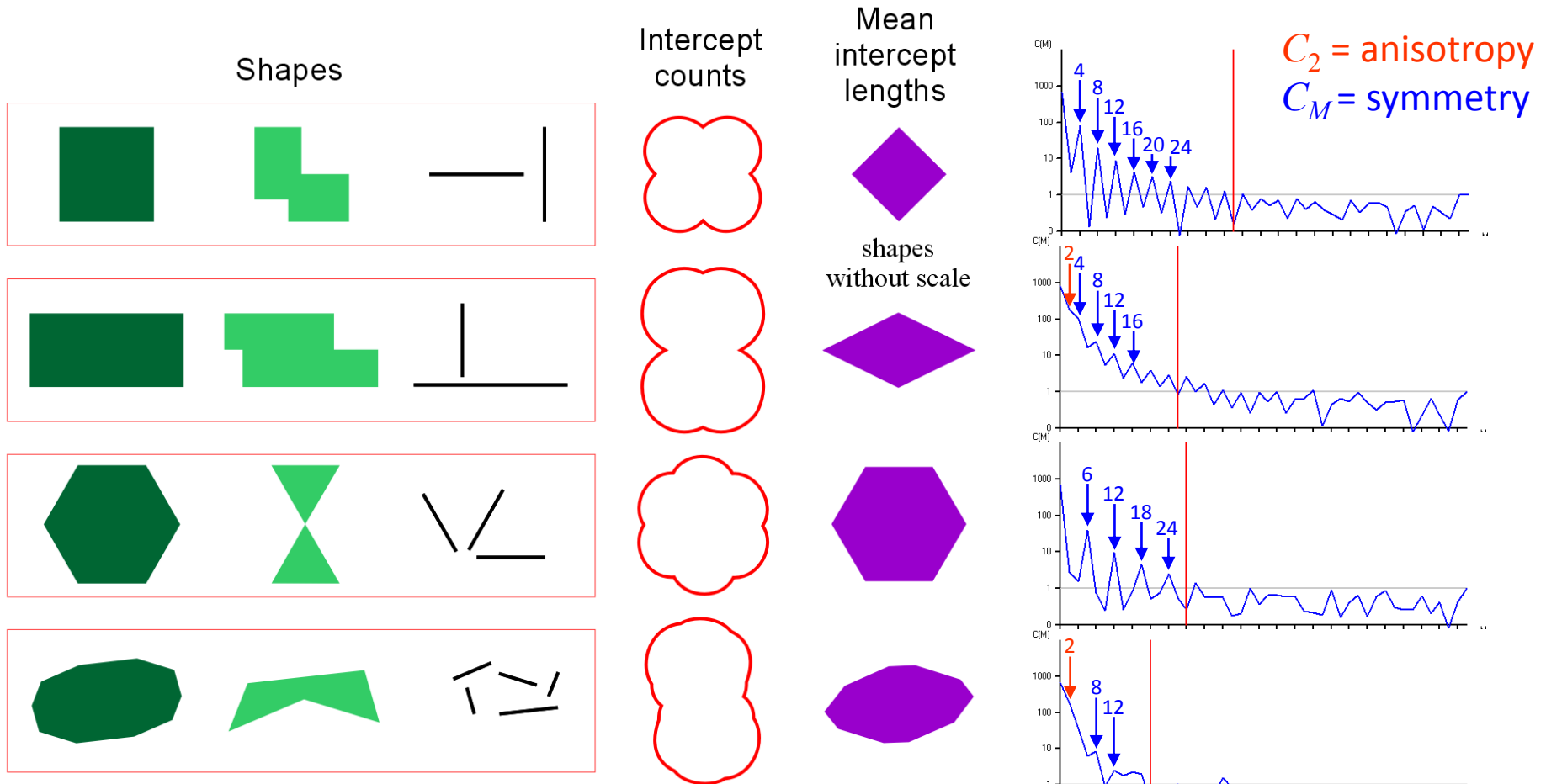
C_M = symmetry

A power spectrum with high C values on harmonics 6, 12, 18, 24 characterizes symmetry of order 3 and 6

Launeau & Robin (1996)

23

A power spectrum with high C values on harmonics 10 and 20 characterizes symmetry of order 5 such as the pentagon below
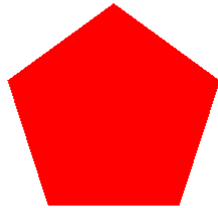
C$_2$ = anisotropy
C$_M$ = symmetry
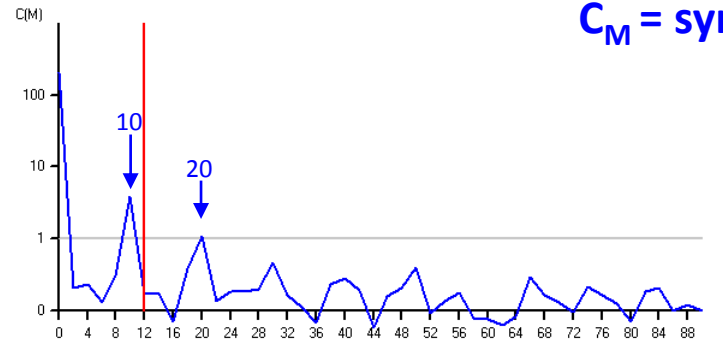
A a=0,5060 cm b=0,5072 cm R=0,998 , 80,42°

(1) 126°
(2) 163°
(3) 19°
(4) 54°
(5) 89°
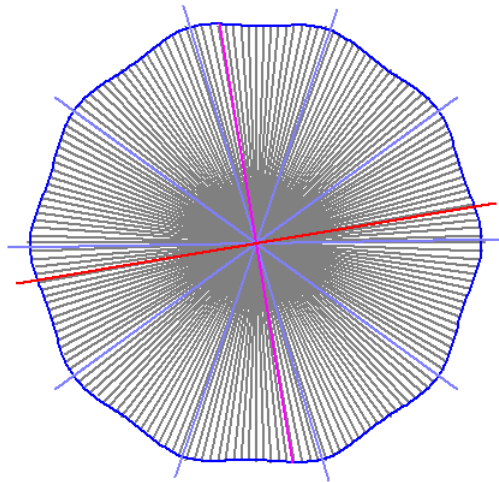
A NIa=0,138 cm-¹ NIb=0,137 cm-¹ R=0,998 , 80,42°

(1) 90°
(2) 126°
(3) 163°
(4) 18°
(5) 54°

0,1 cm

24
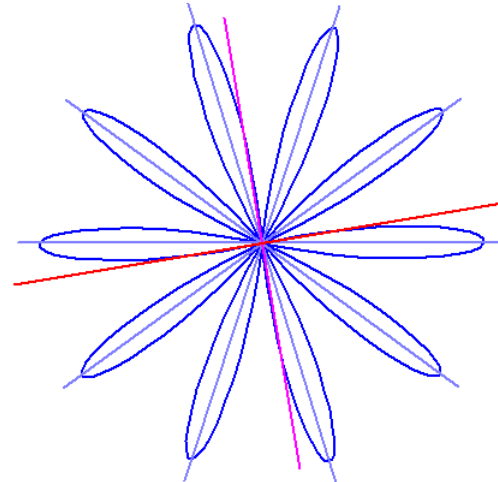
In 2D image, the inertia tensor always gives the exact size of one ellipse. The size of a and b of one rectangle is enlarged and its exact size is better given by the bounding box values a_{box} and b_{box}.

In 2D, intercepts are mean values calculated on A/J lines with J the interline size. Thus, the mean diameter of one ellipse is:

$$L_{max}(\alpha) = \frac{4}{\pi} \cdot \bar{L}(\alpha) = \frac{4}{\pi} \cdot I.\bar{N}_L(\alpha) = \frac{A}{J} \cdot \sum_{j=1}^{A/J-1} N_{Lj}(\alpha)$$

I sampling interval on line
J interline size

In case of an **ellipse**, the size of each mean length of intercepts must be multiplied by **4/π**.
This is not the case for a rectangle.

Launeau & Robin (1996)

inertia tensor

a=312.493 pxl b=156.780 pxl R=1.993 α=90.00°
a_{box}=313 pxl b_{box}=157 pxl

a=361.415 pxl a=181.284 pxl R=1.994 α=90.00°
a_{box}=313 pxl b_{box}=157 pxl

100 pxl

intercepts

$\delta\alpha = 2° \rightarrow K = 90$
$I = 1\,pxl$
$J = 2\,pxl$

$C_0 + C_2$ = 98.1% ellipse data

Notes the characteristic distribution of C_M for the rectangle

a=305.027 pxl b=156.256 pxl R=1.952 α=89.96°
a=239.568 pxl b=122.723 pxl

a=390.703 pxl b=198.634 pxl R=1.967 α=90.05°
a=306.858 pxl b=156.006 pxl

4/π

100 pxl
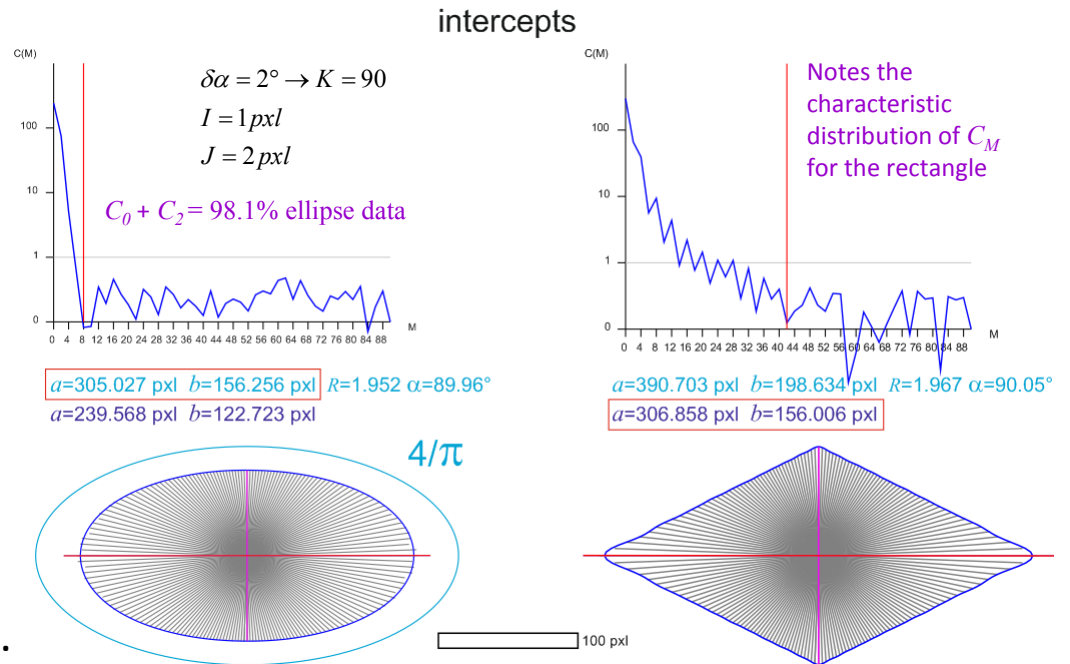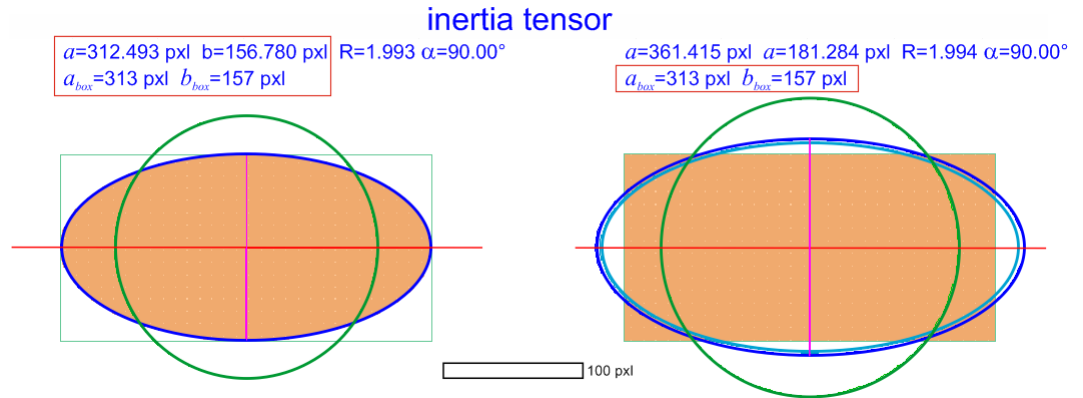
Shape Preferred Orientation (OCW-UN-SPO) Launeau P. 2017

Anisotropy	Inertia tensor	<u>Mean</u> intercept length

9°

mean L

$L = 0.569$

$L = 0.445$
$L \times 4 / \pi = 0.567$

$L = 0.804$

$L = 0.623$
$L \times 4 / \pi = 0.794$

$L = 1.138$

$L = 0.878$
$L \times 4 / \pi = 1.118$

$L = 2.275$

$L = 1.743$
$L \times 4 / \pi = 2.219$

2°

$L = 1.863$
$L \times 4 / \pi = 2.372$
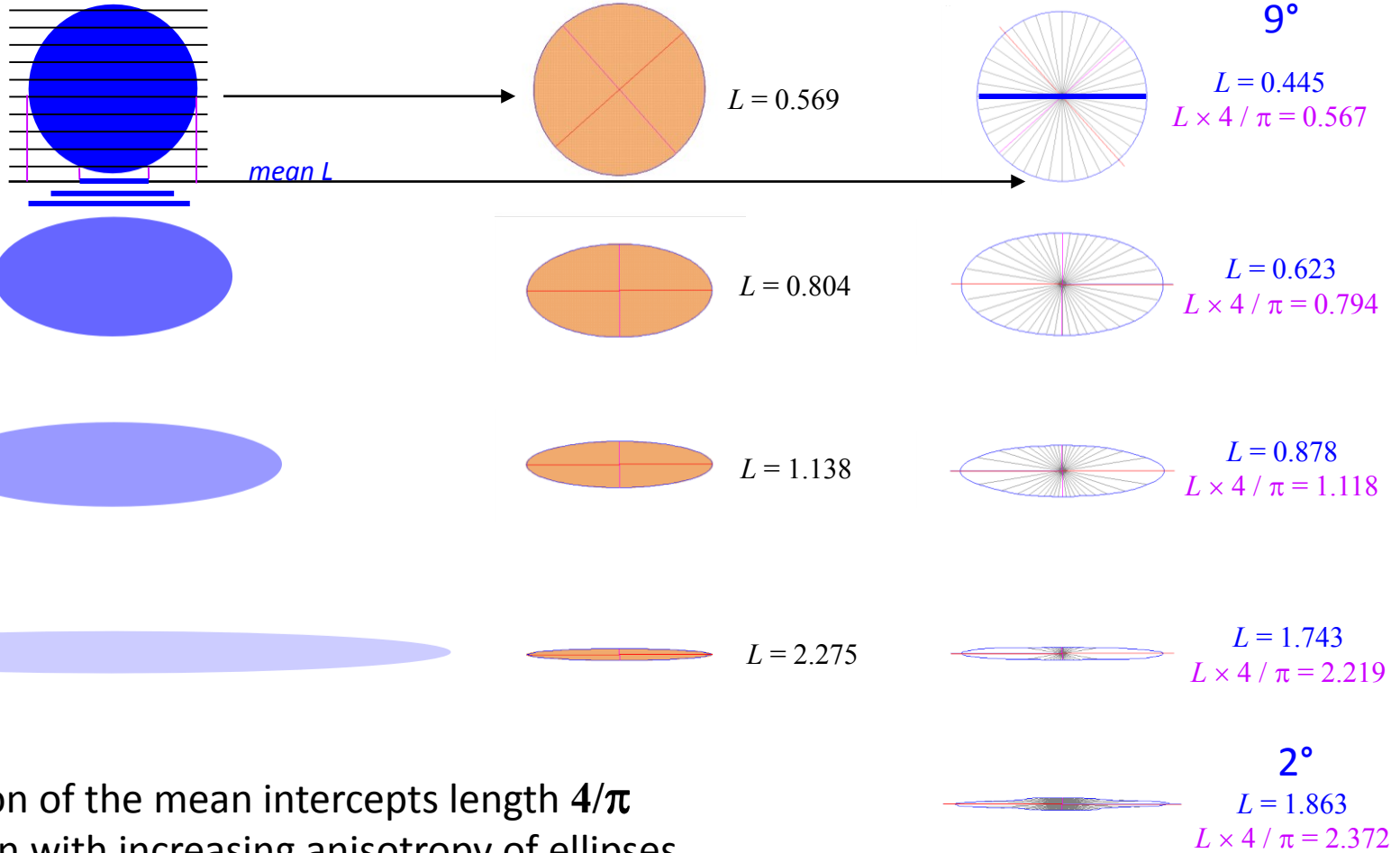
Illustration of the mean intercepts length **4/π**
correction with increasing anisotropy of ellipses

Figures not to scale

Comparison between inertia tensor and intercepts shows that intercepts <mark>underestimate</mark> the SPO intensity of objects presenting sharp boundaries whereas elliptical ones give identical results with both methods.

A n=2 a=5,9926 cm b=3,9318 cm R=1,524 [1,729]n [1,734]b , 89,99°
K=0,398, Kn=0,498 {0,799}, Kb=0,501 {0,795}

$r = 3$ $R = 1.52$

A a=3,9357 cm b=2,5886 cm R=1,520 , 90,12°

(1) 84°

$R = 1.52$

A a=11,9422 cm b=7,8547 cm R=1,520 , 90,12°

(1) 60°   ← Sub-direction detection
(2) 120°
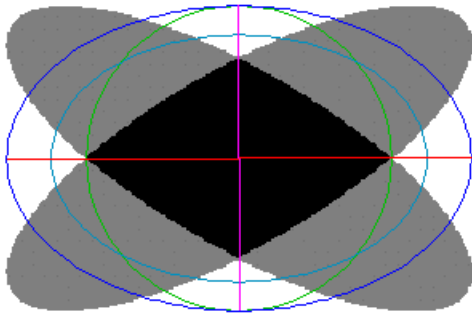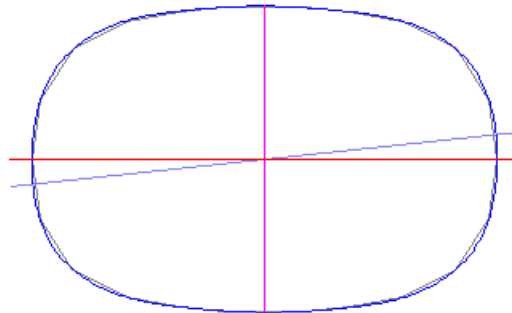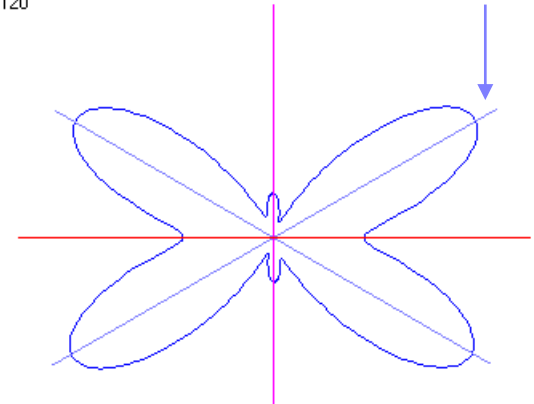
Inertia tensor   **Mean lengths of intercepts**   **Boundaries directions**

A n=2 a=0,4883 cm b=0,3171 cm R=1,540 [1,732]n [1,746]b , 89,82°
K=0,407, Kn=0,500 {0,814}, Kb=0,506 {0,804}

$r = 3$ $R = 1.54$

A a=0,2599 cm b=0,1990 cm R=1,306 , 89,98°

(1) 61°
(2) 117°

<mark>$R = 1.30$</mark>

A a=0,9649 cm b=0,7434 cm R=1,298 , 89,98°

(1) 23°
(2) 63°
(3) 117°
(4) 158°

a_2 b_1 a_1

b_2

27
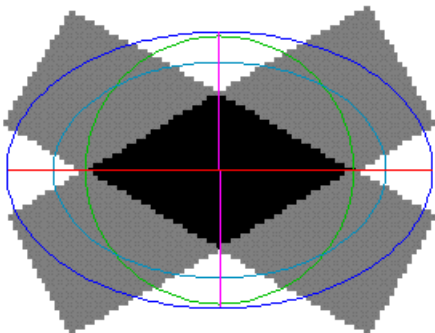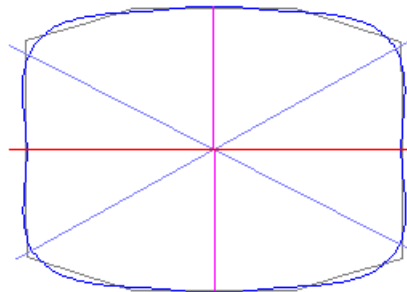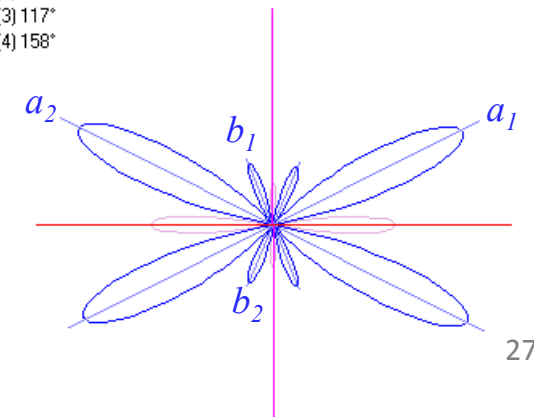
Roses diagrams of directions can be useful for the detection of SPO imbrication of 2 populations of objects, like rectangles and ellipses or for the detection of diamond shapes characterized by boundary directions aligned along S and C planes.
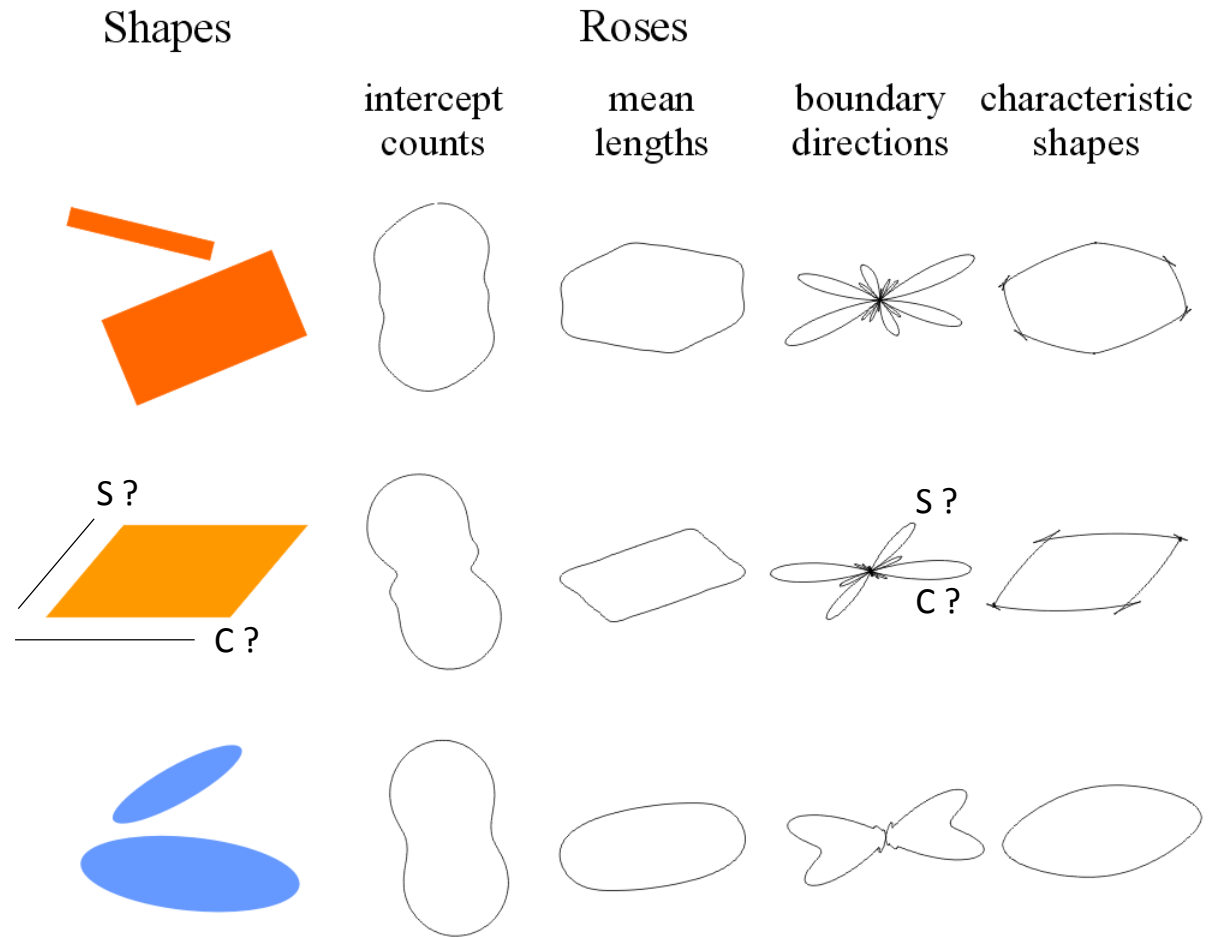
Such observations however can not be used in 3D SPO construction by combination of 2D SPO measurements which must be ellipses.

The inertia tensor is centered on the gravity center and can be represented as an ellipse with long radius a and short radius b enclosing the object, including irregular boundaries enlarging its footprint in the image. It is then possible to resize an ellipse, or eventually a disk, to the effective surface area of the object.

A scan along the main axis direction and its perpendicular direction also allows the drawing of a bounding box enclosing all the pixel of the object.

Inertia tensor

Ellipse with identical surface area

Disk with identical surface area

D_A

$2a_{box}$

$2a$

$2b$

$2b_{box}$

Rectangular bounding box

The theoretical area of an ellipse is : $A_{ellipse} = \pi \cdot a_{ellipse} \cdot b_{ellipse}$

A is the area of an object. Their ratio allows the definition of the index of deviation from ellipticity:

$$e_{elli} = \frac{\pi \cdot a_{ellipse} \cdot b_{ellipse}}{A_{object}} - 1$$

$$e_{box} = \frac{\pi \cdot a_{box} \cdot b_{box}}{A_{box}} - 1$$

0	2,1	8,9	23,5

Rink (1976)
Launeau (2004)

29
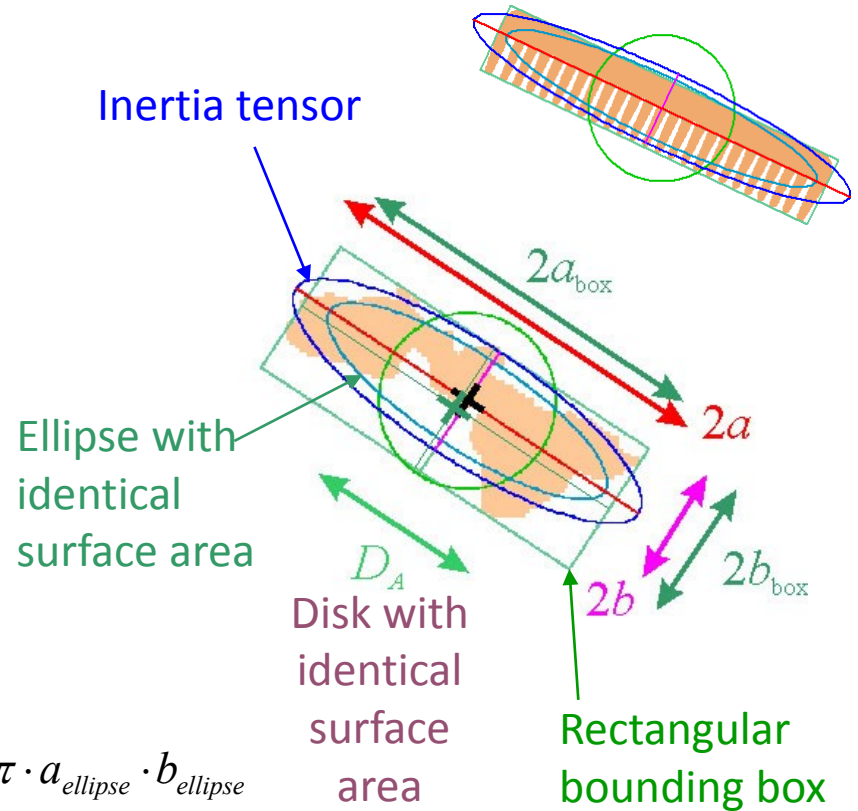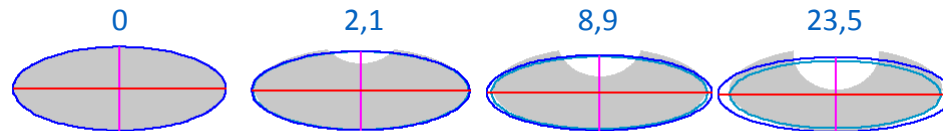
Shape #

Let define 4 shapes with :
1) sharp boundaries (rectangle)
2) smooth boundaries (ellipse – homeomorphic deformation of a circle)
3) centrifugal distribution of pixels more abundant towards both ends
4) centripetal distribution of pixels more abundant towards the gravity center

In all cases, the inertia tensor method always provides the right shape ratio whatever is shape type.
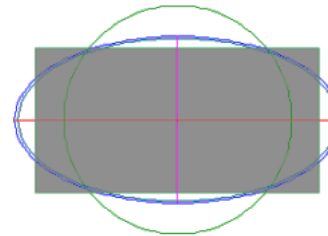
1 : rectangle

$r = 2$
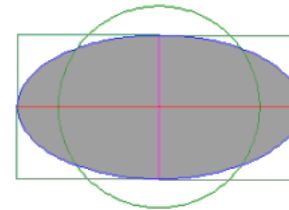
2 : **ellipse**

$r = 2$
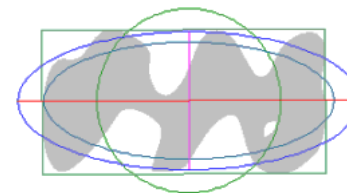
3 : *centrifugal shape*

$r = 2.5$
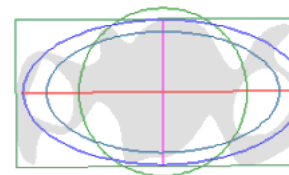
4 : *centripetal shape*

$r = 2$

Launeau (2004)

The analysis of the different shape types by the intercepts method shows a lot of variations in mean length of intercepts or traverses with the scanline angles.

The ellipse and the rectangle having boundaries oriented in the main direction of anisotropy both shapes correspond to one object. On the contrary, the last shape types display a lot of boundaries oblique on the main direction of anisotropy and could be seen as aggregates of sub-objects.

Disk with identical surface area comparison to mean length traverses size distributions

Launeau (2004)
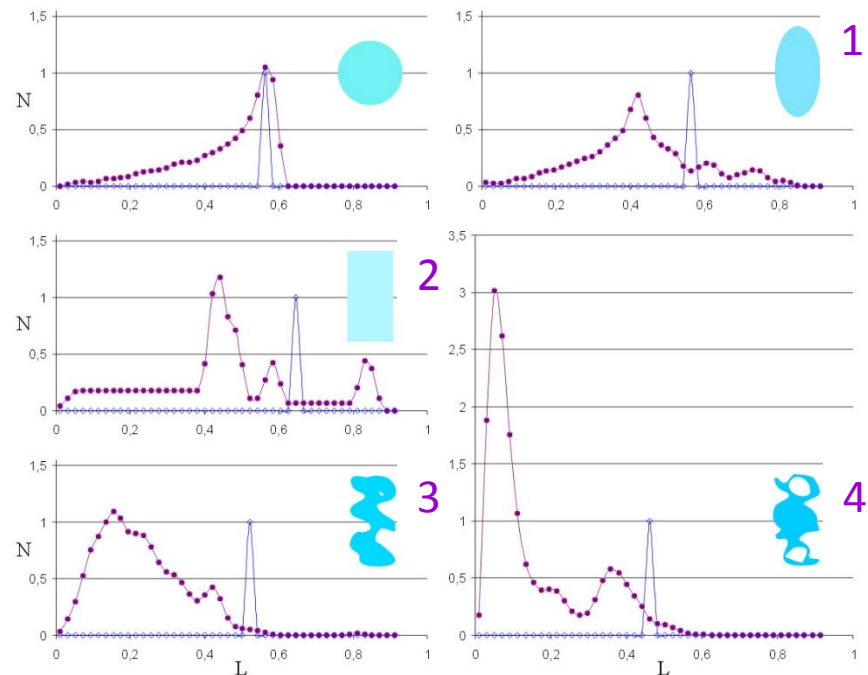
In case of low population the shape type may influence the SPO. Column (a) contains only the object orientation at 60° in row (1), 120° in row (2) and both orientations in row (3). Column (b) to (e) contain the inertia tensor analysis of all shape types. The individual shape ratio r is identical in line (1) and (2). The SPO of 2 objects in line (3) display intensities R proportional to individual r. Their normalizations R_n give the expected value given by the PO of the lines in (a, 3).

$$R_n = \sqrt{\frac{1+K_n}{1-K_n}}$$ (see course 02 p. 18)

		1	**2**	**3**	**4**
	a	b	c	d	e
1					
2					
r		2.00	2.00	2.50	1.92
3					
R	1.74	1.36	1.36	1.46	1.34
R_n		1.74	1.74	1.74	1.74
4					
$R_{intercepts}$		1.19 / 1.25	1.37	1.17	1.12

In line (4) the mean length of traverses gives the right SPO intensity in (c) for the ellipses. This intensity is underestimated in the case (b) of the rectangles. The results are quite different in column (d) and (e). The intercepts method clearly detects the orientation of sub-objects hidden in the aggregates.

Launeau (2004)
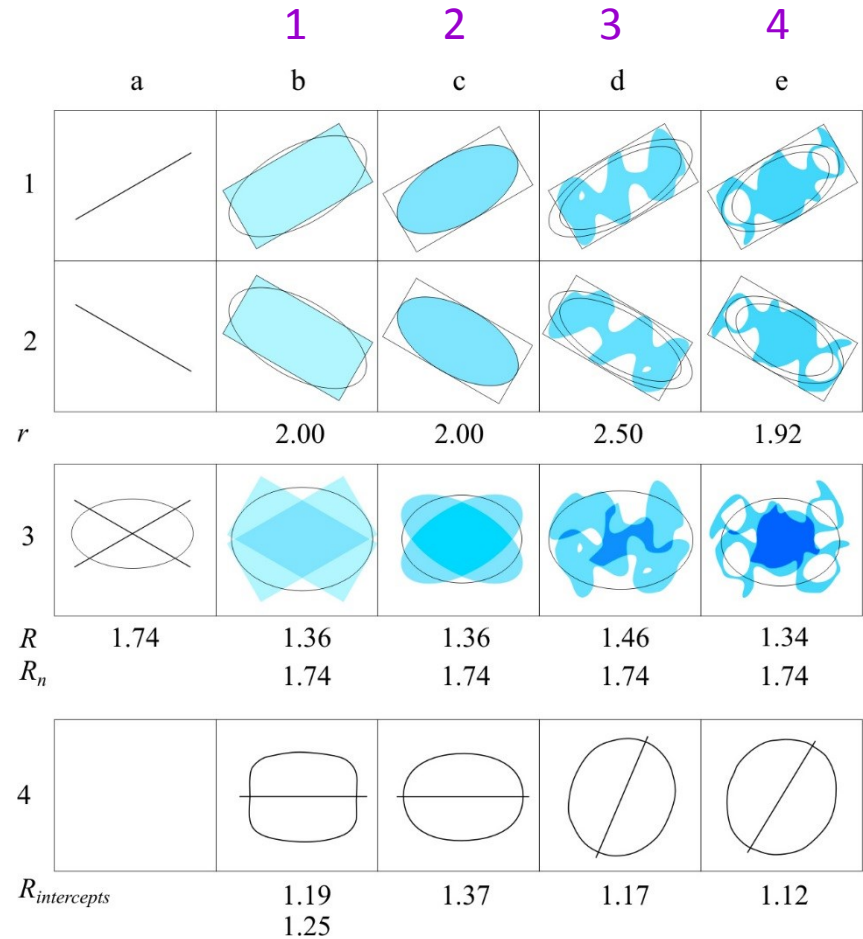
Let deform passively a set of 24 shape types initially oriented every 10°. The inertia tensors of all shape type populations display the same initial SPO R=1 and final SPO R=2. **Whatever is the individual shape**, the inertia tensor of a population records the **strain** intensity while each population has an initial isotropic angular distribution of objects.

$$1/\sqrt{\lambda_1} \qquad \lambda_1 = 2$$

$$\sqrt{\lambda_1}$$

Passive isosurface deformation

Shape # 1234	1	2	3	4

Pixel density
100%
75%
50%
25%
0%

Not display at the same scale

R	1.00	1.00	1.00	1.00	1.00
R	1.99	1.99	1.98	1.99	1.99

33
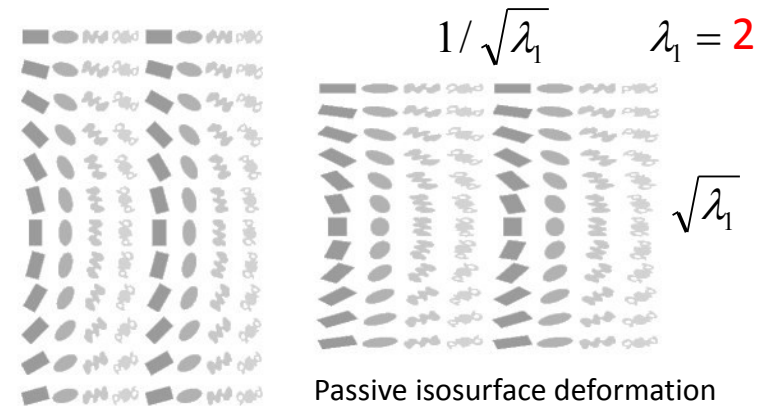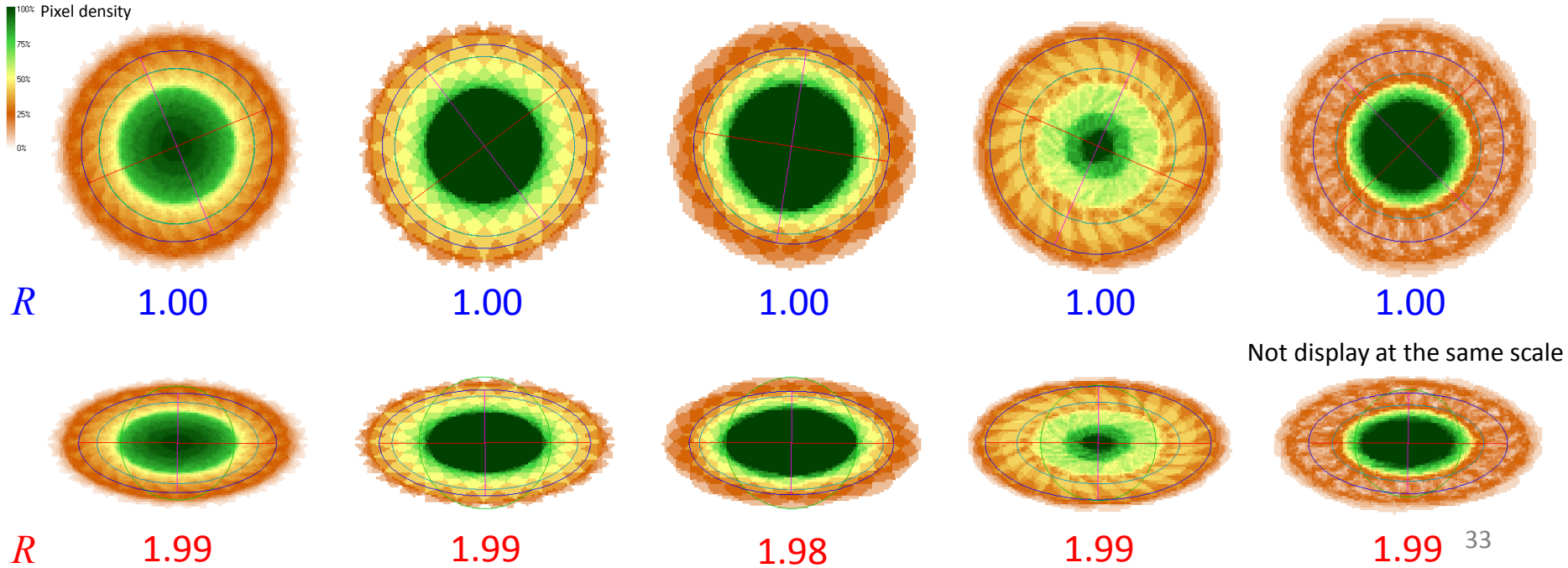
The intercepts of all shape type populations display the same initial SPO R=1 and final SPO R=2. **Whatever is the individual shape**, the intercepts of a population records the **strain** intensity of a passive deformation while that population has an initial isotropic angular distribution of objects.

$$1/\sqrt{\lambda_1} \qquad \lambda_1 = 2$$

$$\sqrt{\lambda_1}$$

Passive isosurface deformation
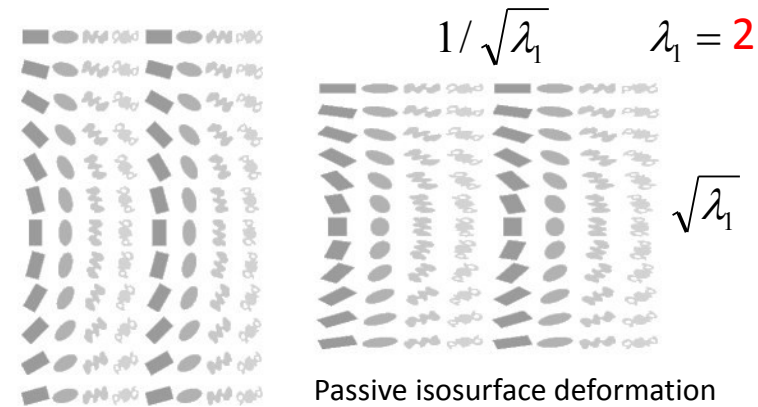
Shape # 1234   1   2   3   4

A B C D a=0,2856 cm b=0,2838 cm R=1,007 , 101,05°

(1) 90°
(2) 148°
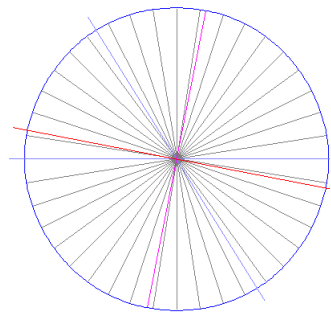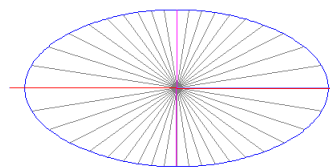
A a=0,4402 cm b=0,4397 cm R=1,001 , 56,18°

(1) 176°
(2) 83°
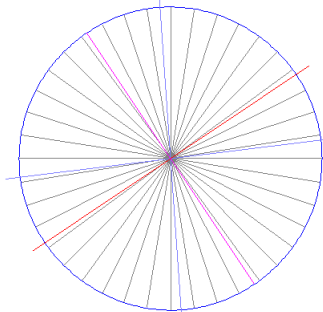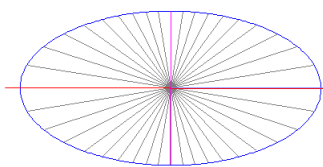
B a=0,4200 cm b=0,4191 cm R=1,002 , 138,64°

(1) 140°
(2) 32°
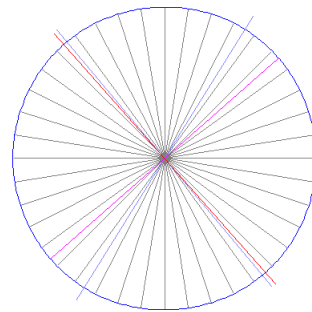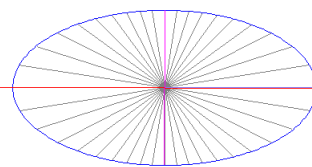
C a=0,2343 cm b=0,2314 cm R=1,013 , 100,27°

(1) 90°
(2) 149°
(3) 30°
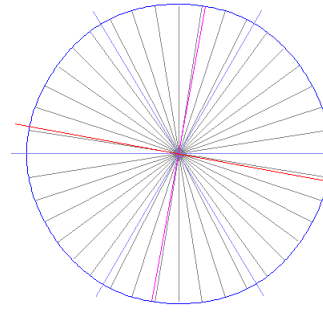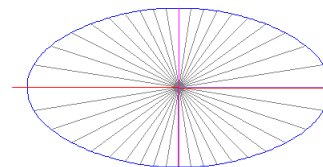
D a=0,1570 cm b=0,1555 cm R=1,010 , 101,31°

(1) 91°
(2) 145°
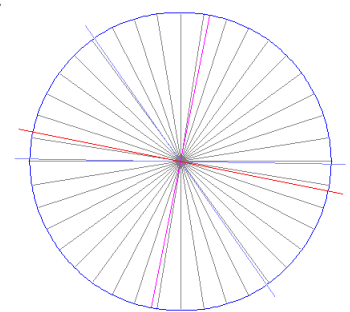
R 1.01   1.00   1.00   1.01   1.01

Not display at the same scale
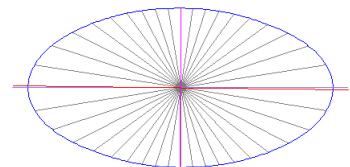
R 1.93   1.96   1.96   1.91   1.92

34

Let now deform actively, by rigid body rotation in simple shear up to the critical γ_c, the same set of 24 shape types initially oriented every 10°. $Rf = r^2$ and $R_n = r$ at γ_c.

Whatever is the individual shape, the inertia tensor of a population records the **SPO** intensity R weighted to the mean individual r while that population has an initial isotropic angular distribution of objects. When r is known R_n allows the estimation of the full SPO intensity.
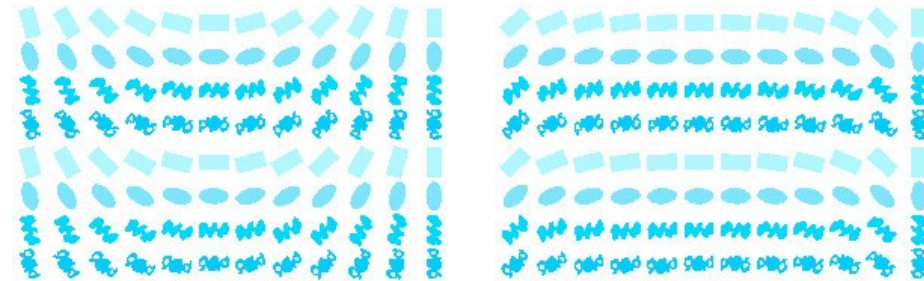
$r = 2$
$\gamma_c = 3.93$

Shape # 1234	1	2	3	4
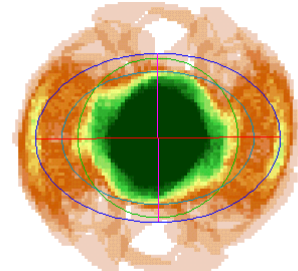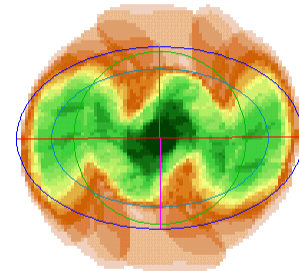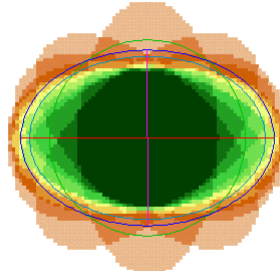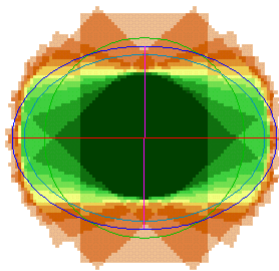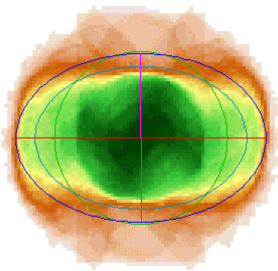
$R\gamma_c$	1.48	1.44	1.44	1.57	1.44
R_n	1.99	1.95	1.98	1.95	1.99
r	2.08	1.97	1.98	2.49	1.90

$$K = \frac{R^2 - 1}{R^2 + 1} \quad k = \frac{r^2 - 1}{r^2 + 1} \quad K_n = K/k \quad R_n = \sqrt{\frac{1 + K_n}{1 - K_n}}$$ (see course 02 p. 18)

35

$Rf = r^2$ and $R_n = r$ at the critical shear rate γ_c for which most of the objects are parallel to the simple shear flow plan.

Population of parallel objects display angular distribution of boundaries similar to the individual objects angular distribution of boundaries which has a strong impact on intercepts SPO. Ellipse, homeomorphic deformation of a disk, and rectangles are the only shape type fully compatible with flow quantification.
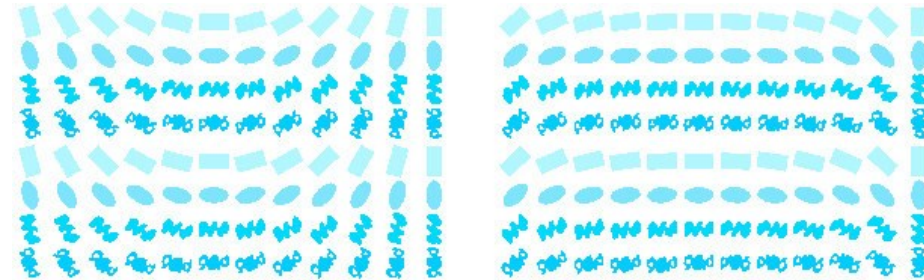
$r = 2$
$\gamma_c = 3.93$

This shapes are aggregates of oblique grains

Shape # 1234	1	2	3	4
$R\gamma_c$ 1.12	1.33	1.47	1.19	1.12
R_n 1.19	1.68	2.04	1.27	1.23
r 2.08	1.97	1.98	2.49	1.90
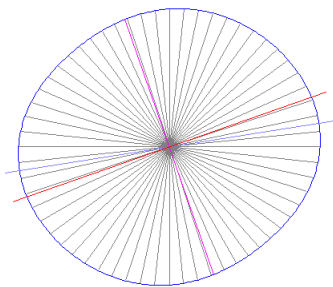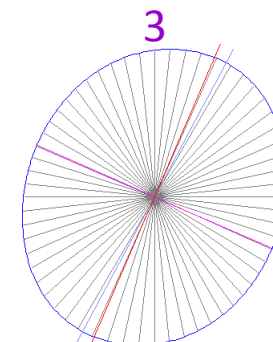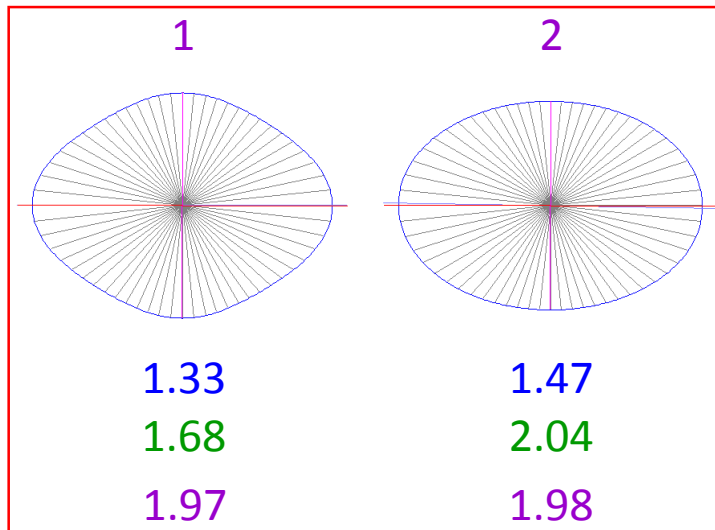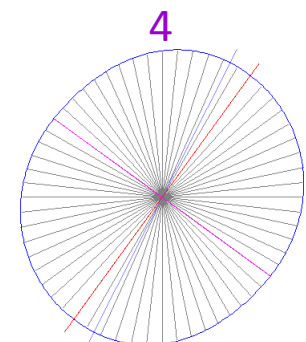
$$K = \frac{R^2 - 1}{R^2 + 1} \quad k = \frac{r^2 - 1}{r^2 + 1} \quad K_n = K/k \quad R_n = \sqrt{\frac{1 + K_n}{1 - K_n}}$$ (see course 02 p. 18)

36

The following example is the drawing of a quartzite thin section where cut grains are masked in cyan. Since boundaries occupy some surface it is necessary to include them in the calculation of the quartz modal fraction which should be 100% in a quartzite.
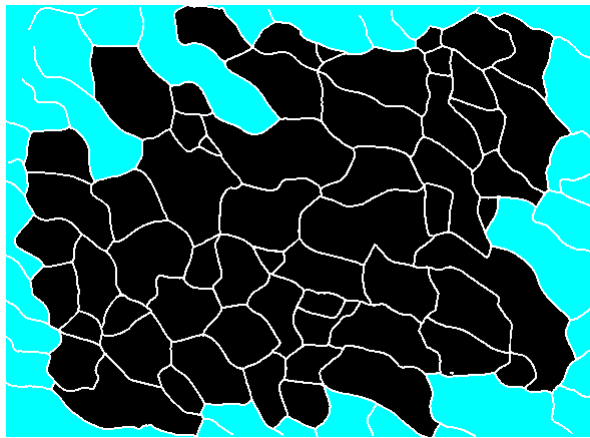
60 objects
89.1% black grains
93.7% black grains + borders
28.4% cyan masked grains

$$A_{quartz\%} = A_{black+border} \big/ \left(A_{image} - A_{green+border} \right)$$

A n=60 a=0,0865 cm b=0,0604 cm R=1,433 [2,195]n [2,539]b , 123,67°
K=0,345, Kn=0,656 {0,525}, Kbn=0,731 {0,471}

Pixel density

R = 1.43
α = 123.7
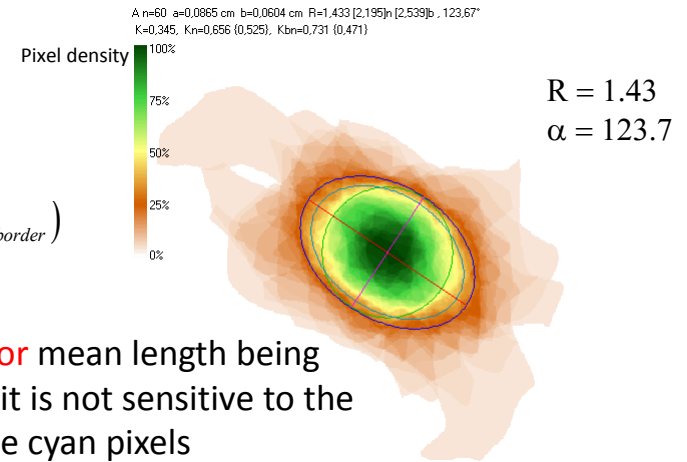
The weighted inertia tensor mean length being calculated on black pixels it is not sensitive to the presence or absence of the cyan pixels

When cut objects have been deleted the definition of a mask of measurement eroded with half of the average grain size allows the retrieval of the right modal fraction
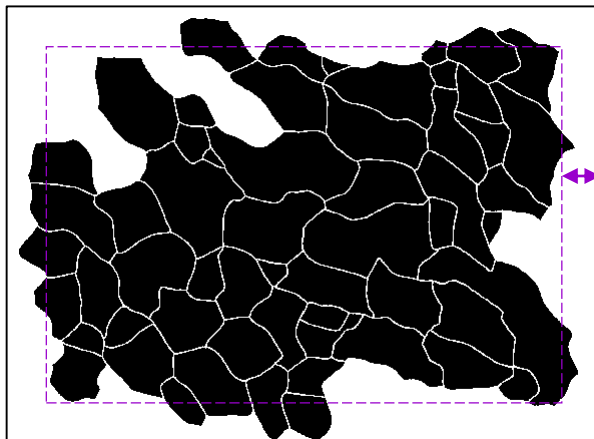
60 objects
67.1 % black grains + borders
95.9% black grains + borders + average

Mean size / 2

$$A_{quartz\%} = A_{black+border} \big/ A_{erode\_image}$$

A n=60 a=1,4645   b=1,1119   R=1,317 [1,759]n [1,911]b , 125,03°
K=0,269, Kn=0,511 {0,525}, Kbn=0,570 {0,471}

R = 1.32
α = 125.0
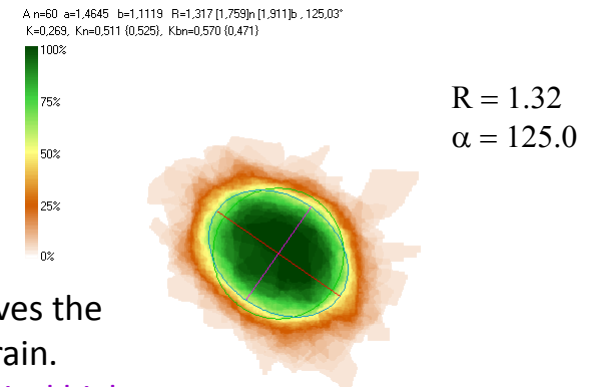
The unweighted inertia tensor gives the same statistical weight to each grain.
Both stacks of pixels display elliptical high density suitable for 3D estimation.

Drawing modified from Quartzite thin section from Ramsay and Huber (1983, page 118)

37

The intercepts method do not necessitate the deletion of cut objects when the procedure stop the detection of intercepts along images borders
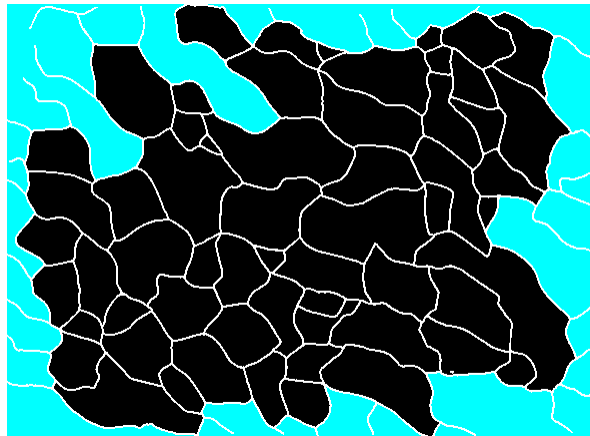
60 objects
66 % black grains
28 % cyan masked grains
94 % quartz + 6% borders

The unweighted inertia tensor gives results between both intercepts mean length:
$R = 1.32$
$\alpha = 125.0$

The weighted inertia tensor gives higher values because of the presence of a few large grains: $R = 1.43$
$\alpha = 123.7$

A B a=0,6989 mm b=0,5122 mm R=1,365 , 124,47°

(1) 125°

Mean length intercepts of black and cyan classes
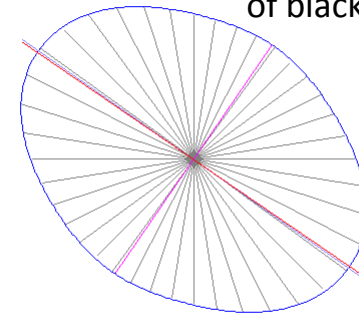
$R = 1.37$
$\alpha = 124.5$

A a=0,6586 mm b=0,5059 mm R=1,302 , 125,39°

(1) 126°

Mean length intercepts of black class only

$R = 1.30$
$\alpha = 125.4$

0,1 mm

Intercept detection on both classes (green for black and red for cyan)
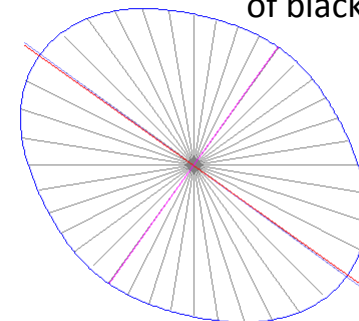
The measurement mask, set to a quarter of the image, scan from position 1 to 9 over it allows a quantification of the results invariance by translation. It gives 9 SPO whose R and α standard deviations characterize the results homogeneity through the whole image.
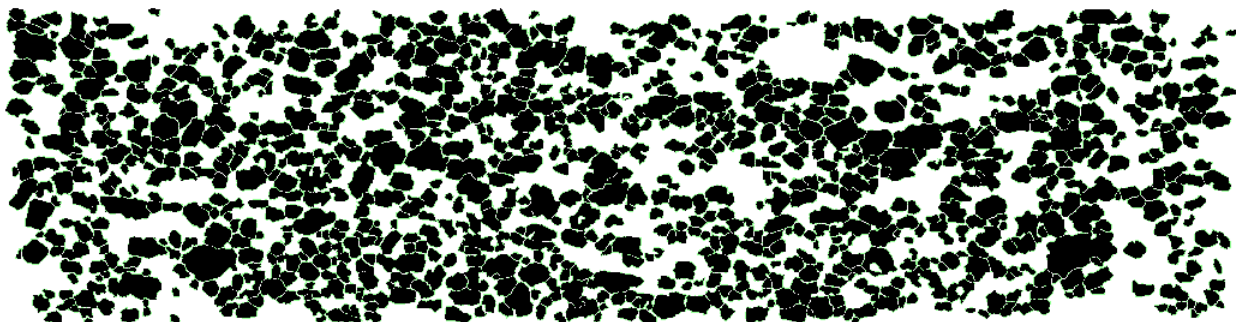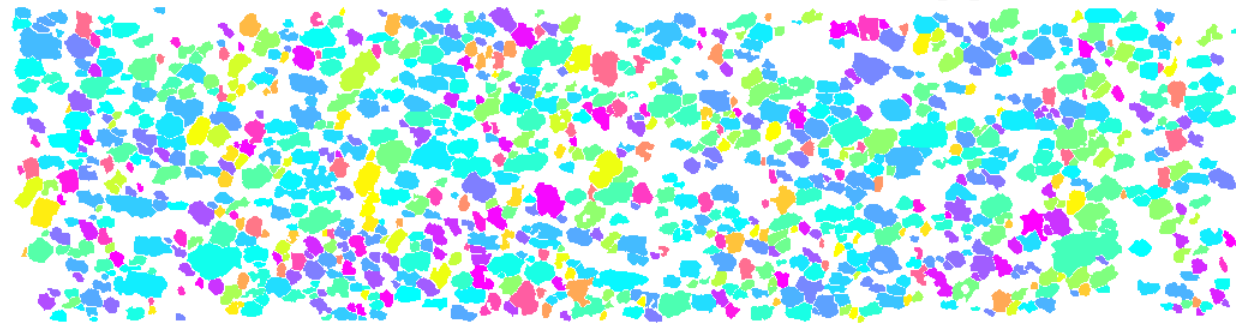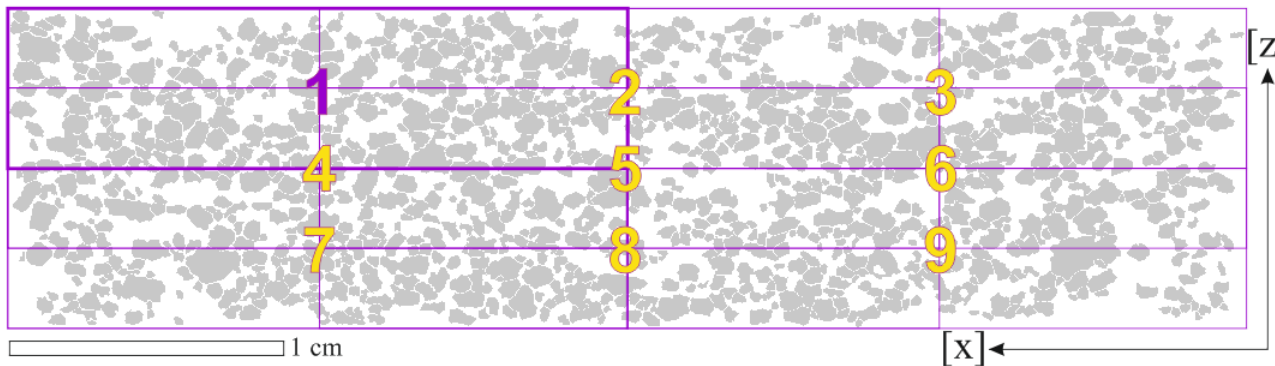
inertia tensors

A n=949 a=0,0723 cm b=0,0561 cm
R=1,288 [1,894]n [2,142]b , 89,66° , angle X : 179,66°
K=0,248, Kn=0,564 {0,439}, Kbn=0,642 {0,386}

Pixel density
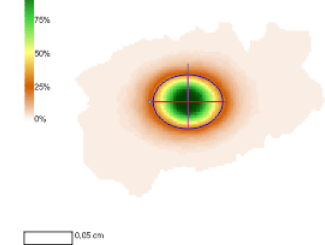
[z]

[x]

1 cm

0,05 cm

±1σ

A n=949 a=0,0723 cm b=0,0561 cm
R=1,288 [1,894]n [2,142]b , 89,66° angle X : 179,66°
K=0,248, Kn=0,564 {0,439}, Kbn=0,642 {0,386}

R = 1.29 ± 0.02

α = 89.7 ± 2.7
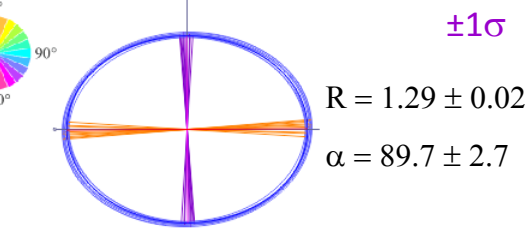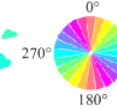
0,05 cm

intercepts

A a=0,0853 cm b=0,0755 cm
R=1,130 , 87,10° , angle X : 177,10°

(1) 89°

R = 1.13 ± 0.02

α = 87.1 ± 2.1

0,05 cm

39

Launeau & Robin (2005)
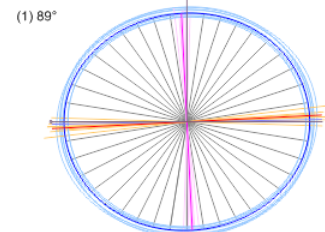
The order of crystallization also play a role in the formation of mineral SPO like in this example from a gabbronorite of the Bushveld (South Africa)

The first mineral OPX presents automorphic crystals with a compact shapes characterized by a low deviation index to the ellipticity. The plagioclase continuing to crystallize after the OPX it display overgrowth poecilitic shapes and strong deviation index to the ellipticity. The last mineral CPX occupies the last free gaps between other minerals.

In this case, OPX is the only mineral recording the magma flow whereas plagioclase and CPX present less significant mixed SPO.

Launeau (2004)

orthopyroxene   plagioclase   clinopyroxene

$$e_{ellipse} = \frac{\pi \cdot a \cdot b}{A} - 1$$

ellipticity   pixel density

SPO

PO

40
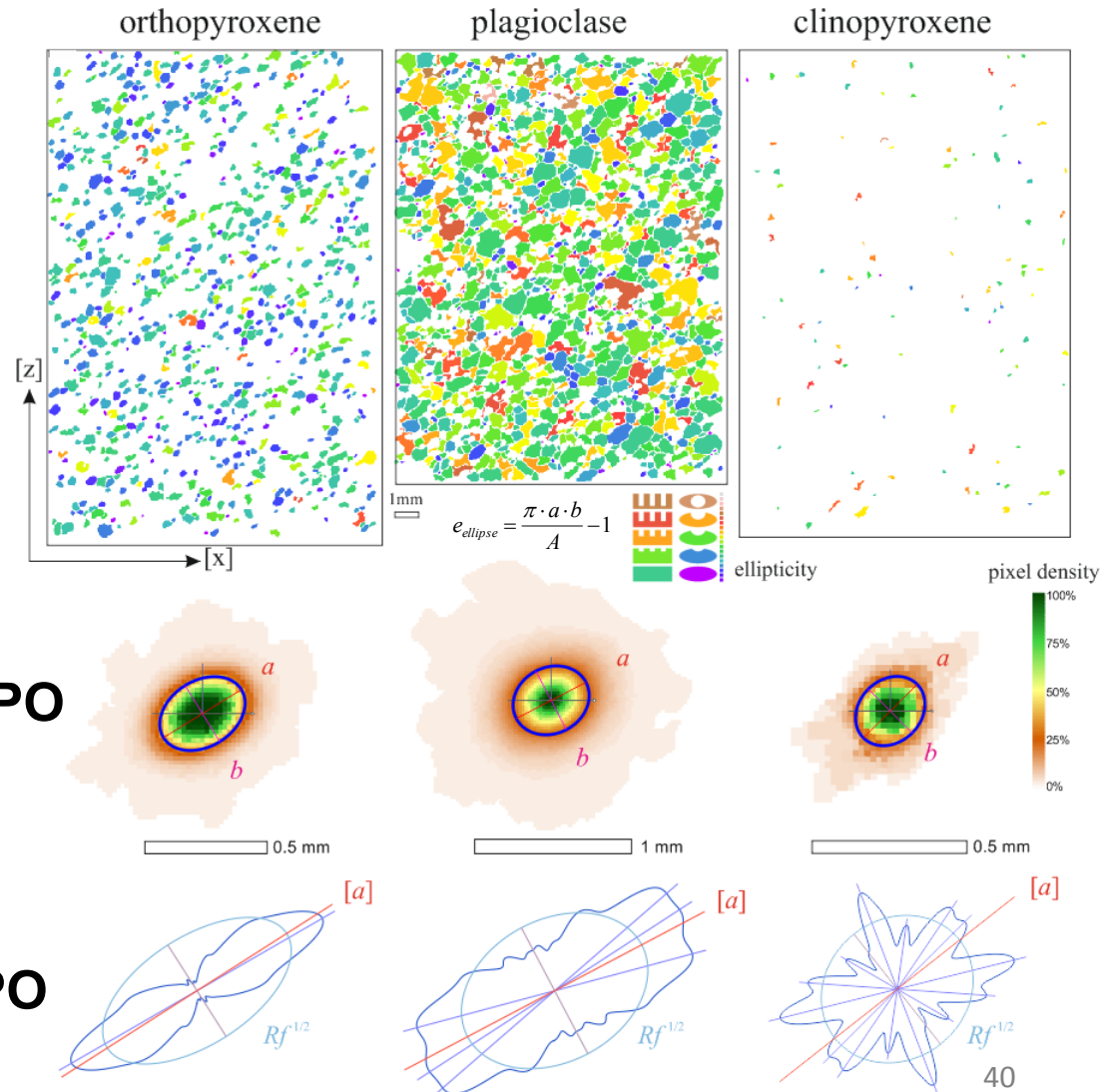
Comparison with spatial distribution using center to center or Fry (1979) diagrams

The center to center method compile all the distances between each object gravity center and all its neighboring object gravity center. When all objects are identical to each other the minimum distance draw exactly 2 times the mean object.

a   b   c   d
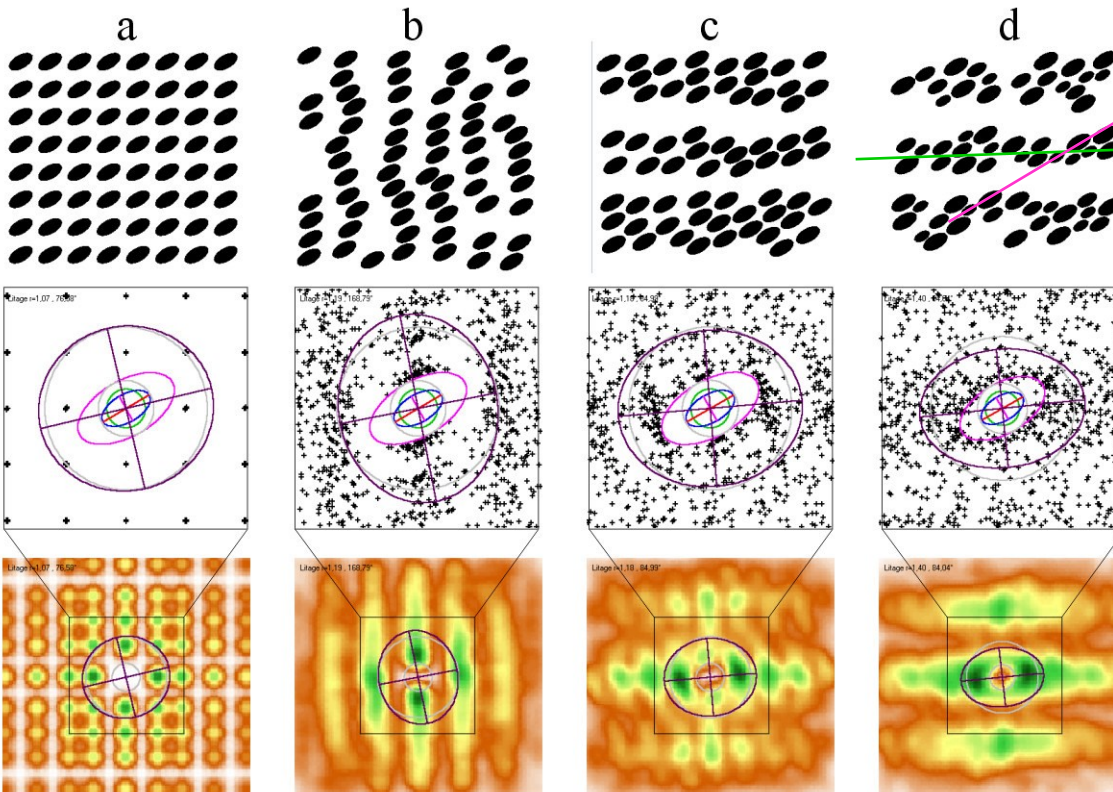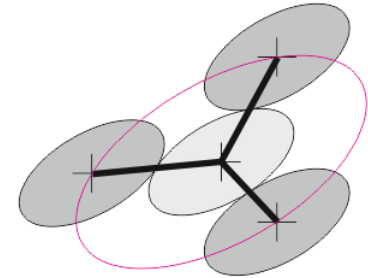
SPO

layering

$Rf = \infty$ $K = 1$ $R = 2$

Parallel objects present infinite PO and SPO equal to the mean object

SPO2003 uses low-pass filters and a color palette to facilitate the analysis of the spatial distribution which are efficient to reveal the presence of bedding or layering independently of the SPO.

41

Image borders induce density attenuation along them.

This sensitivity to boundary is avoided by setting a window of starting centers, from where neighboring centers are searched in a disk having a radius equal do the gap between image boundary and that starting window.

sensitive to boundary

not sensitive to boundary

+ symmetry
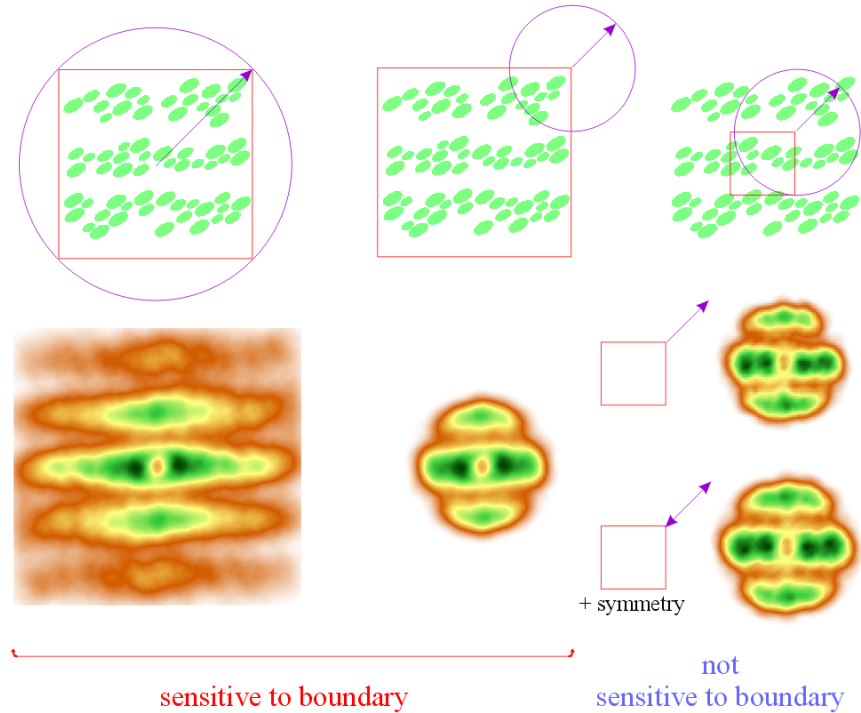
Spatial distribution and Compaction

C 0.88 S 0.42 R 0.62

C 0.88 S 0.42 R 0.62

C 0.88 S 0.42 R 0.62

C 0.75 S 0.50 R 0.72

C 0.41 S 0.90 R 1.32

C 0.59 S 0.63 R 0.91
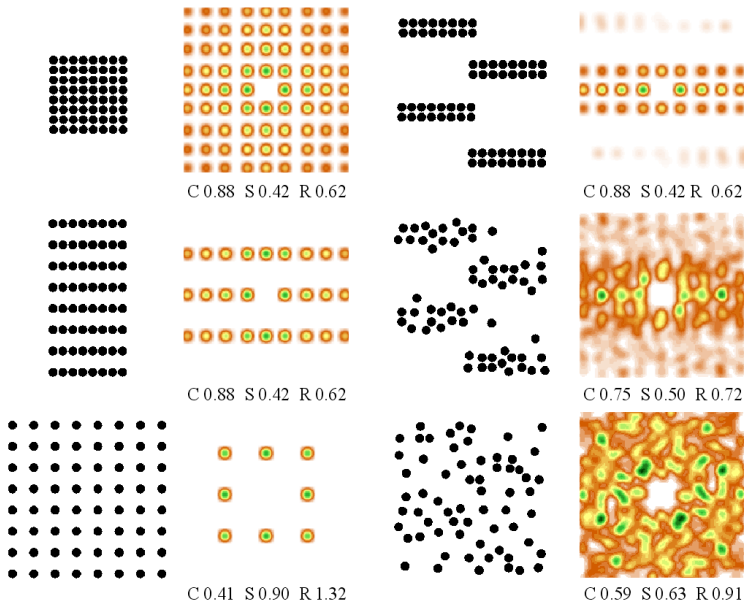
Examples of compaction, scattering and homogeneity analysis (see SPO2003 center-center).

Example of comparable estimations of a strain by Fry diagram, mean intercepts length and inertia tensor

Drawing modified from ironstone oolite thin section from Ramsay and Huber (1983, p. 112 and 120)   R= 1.7 @ 120°

(1) 115°
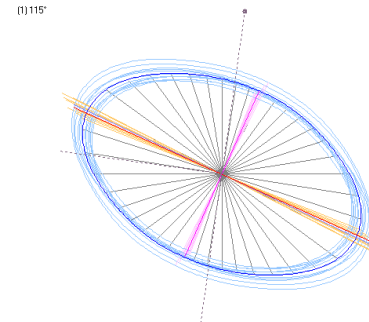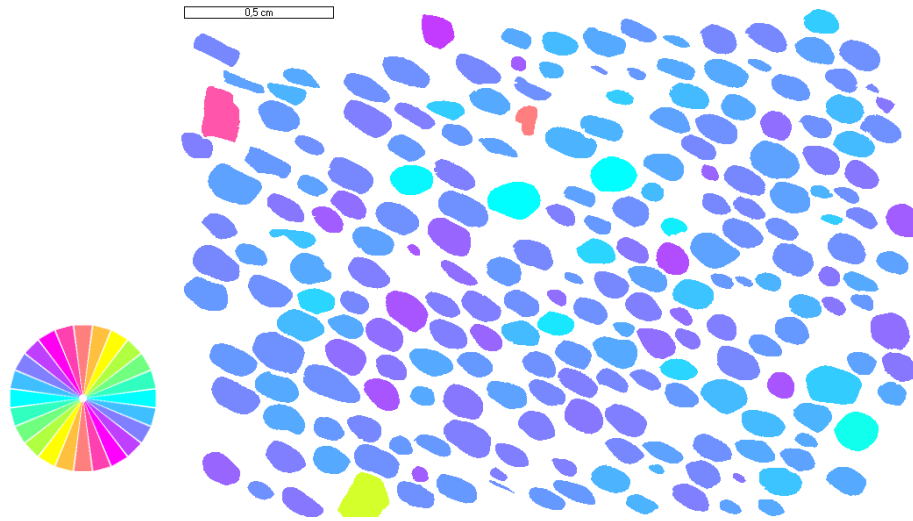
Mean intercept length

R= 1.630 @ 114,3°

1mm

R= 1.645 @ 114,1°

Inertia tensor

image

count of intercept

boundary direction

$M=12$
$M=8$
$M=10$

long axis direction

$k=100$
$k=50$

mean intercept length

autocorrelation
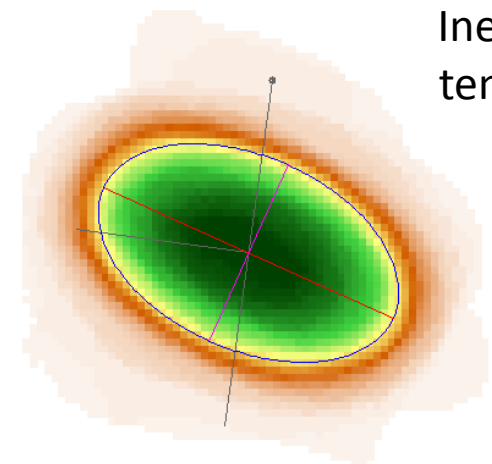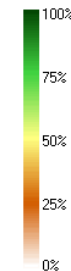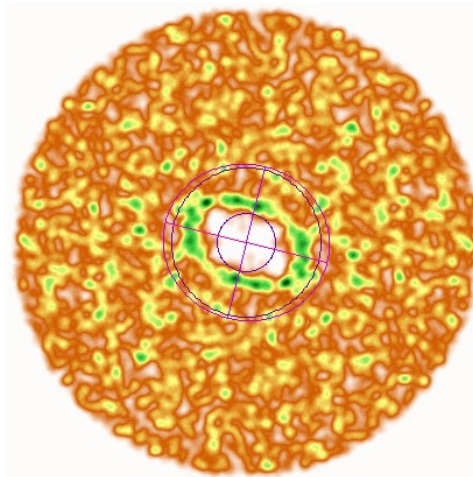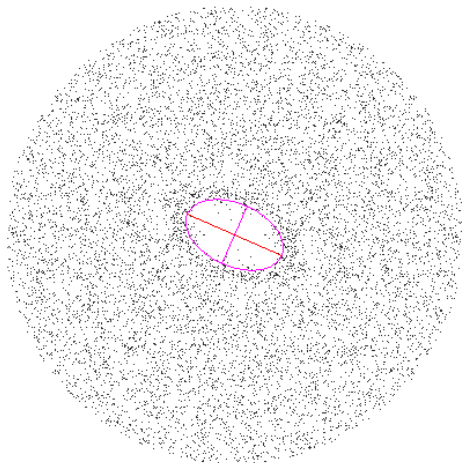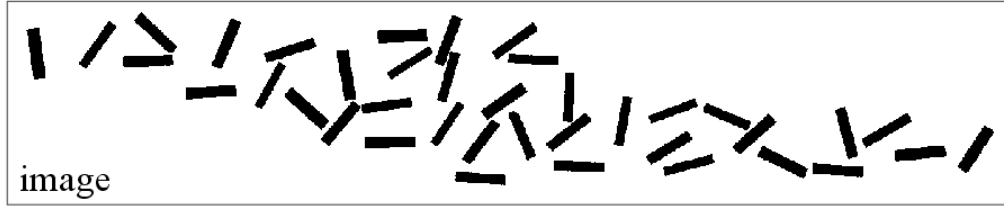
Digitized image of thin rectangular rigid markers floating on a dense viscous liquid which has been deformed in a shear box (Ildefonse et al., 1991). Bulk shear strain of the liquid, $\gamma = 0.94$. Only the analysis of the black rectangles is presented here; they are approximately 25 pixel long.
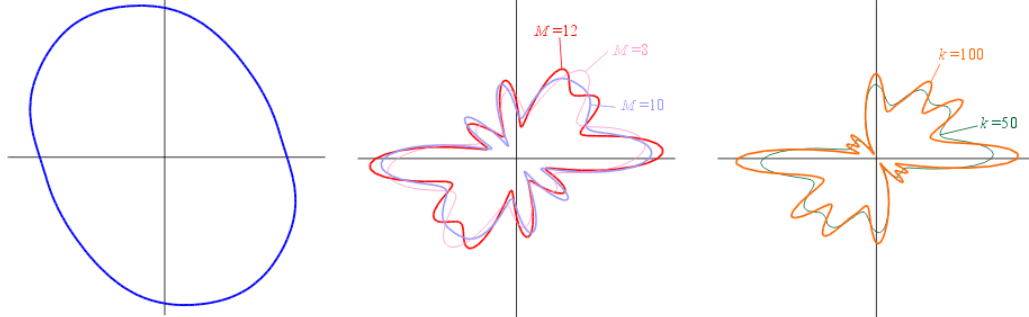
Roses of directions calculated from three Fourier series representations of the rose of intercepts, truncated at the harmonic levels M indicated.

Rose diagrams of the long axes of the rectangular markers, smoothed with the circular Gaussian function $e^{k(\cos\theta - 1)}$ the 2 curves correspond to k = 50 and k = 100.

Launeau et Robin (1996)

The thin lines are contours of the autocorrelation surface calculated from the image with the program AUTO of Pfleiderer et al. (1993). The contour closest to the origin shows mostly the pixel anisotropy, whereas the contours furthest away from the origin, indicate the proximity of some rectangles to each other. The rose of mean intercept lengths calculated from the rose of intercepts, has been scaled to fit between the 5th and the 6th contours away from the origin.

The shearing angle along shell hinges given by the rotation of its initial perpendicular axis of symmetry is classically used for the estimation of the strain of passive deformations. see Ragan (1968) and Ramsay and Huber (1983)

It is shown here that, when tens of objects are available, both inertia tensor and intercepts methods give the same results.

Modified from Ragan, D. M. (1968) p. 30

1.62

1.66

1.59